

The baryogenesis window in the MSSM

B. de Carlos

Centre for Theoretical Physics, University of Sussex
Falmer, Brighton BN1 9QH, UK

and

J.R. Espinosa

Department of Physics and Astronomy, University of Pennsylvania
Philadelphia PA 19104-6396 USA

Abstract

Thermal two-loop QCD corrections associated with light stops have a dramatic effect on the strength of the MSSM electroweak phase transition, making it more strongly first order as required for the viability of electroweak baryogenesis. We perform a perturbative analysis of the transition strength in this model, including these important contributions, extending previous work to arbitrary values of the pseudoscalar Higgs boson mass, m_A . We find a strong enough transition in a region with $2 \lesssim \tan \beta \lesssim 4$ and $m_A \gtrsim 100 \text{ GeV}$, a light Higgs boson with nearly standard couplings, and mass below 80 GeV within the reach of LEP II, and one stop not much heavier than the top quark. In addition, we give a qualitative discussion of the parameter space dependence of the transition strength and comment on the possibility that the transition turns to a crossover for sufficiently large Higgs masses.

1 Introduction

It is by now well established that successful electroweak baryogenesis [1] calls for new physics at the Fermi scale. In the minimal Standard Model (SM) it is not possible to generate a sufficient baryon asymmetry at the electroweak phase transition (EWPHT) because the necessary CP violation is far too small. In addition, the phase transition is at best weakly first order for realistic values of the Higgs mass, and any net $B + L$ number created would be subsequently erased by unsuppressed sphaleron processes in the broken phase. This failure could be an indication that some type of $B - L$ violating new physics is at work above the electroweak scale (see e.g. [2]). Although that is an interesting possibility, we are not really forced to give up the beautiful idea of electroweak baryogenesis, because physics at the 100 GeV scale may not be described by the SM. Supersymmetry (SUSY) [3], the most promising candidate for physics beyond the SM, is expected to be relevant at such energies. Thus, it is natural to examine the prospects for electroweak baryogenesis in models of low-energy SUSY. This is particularly interesting for two reasons; first, because low-energy SUSY is well motivated for reasons not related to the matter asymmetry problem. Second, the parameter regions where electroweak baryogenesis may be successful are in the reach of the present generation of colliders so that the viability of the scenario would be tested in a not too distant future.

Supersymmetric electroweak baryogenesis has been the subject of many studies in recent years. We restrict ourselves to the simplest realization of low-energy SUSY, the Minimal Supersymmetric Standard Model (MSSM). Non-minimal models¹ have also been considered [5].

In SUSY models the presence of extra sources of CP violation [6] besides the Kobayashi-Maskawa angle in the SM can be enough for electroweak baryogenesis and imply CP violating signals on the verge of being seen in upcoming experiments. The observed baryon asymmetry can be accounted for if the new CP violating phases are greater than $10^{-(2-4)}$ and some superpartners are light enough² [7] (see also [8, 9, 10]). In addition, the presence of two Higgs doublets makes possible the spontaneous violation of CP in the Higgs sector at finite temperature [14] (spontaneous breaking does not occur at $T = 0$ for realistic values of the parameters of the model [15]). This mechanism takes place for small values of the pseudoscalar Higgs boson mass m_A and large values of $\tan \beta$ (the ratio of Higgs vevs), and could play an important rôle for electroweak baryogenesis.

The requirement of a sufficiently strong first-order transition to avoid $B + L$ sphaleron erasure of the asymmetry sets a strong upper limit on the mass of some Higgs boson in the theory. Therefore, it is crucial to determine the strength of the electroweak transition and identify the regions of parameter space where it can be strong enough. More precisely, the

¹In models without R -parity conservation, baryogenesis before the EWPHT faces the problem of baryon depletion by the combined action of sphalerons and $B - L$ violating processes. Electroweak baryogenesis offers a particularly appealing solution to this problem, although other possible solutions have been proposed [4].

²These results are affected if the rate of baryon number violation in the high temperature symmetric phase is smaller than it was previously thought to be (see [11, 12, 13]).

requirement is [16]

$$\frac{v(T_c)}{T_c} > 1, \quad (1)$$

where T_c is the critical temperature of the transition, defined by the coexistence of two degenerate minima, and $v = \sqrt{v_1^2 + v_2^2}$, the order parameter of the transition, is the vacuum expectation value (vev) of the Higgs field driving electroweak symmetry breaking (normalized to $v = 246 \text{ GeV}$ at $T = 0$). The first studies of this problem in the MSSM have already pointed out that (1) would require light stops in the spectrum (that is, with masses comparable to the critical temperature of the transition). In ref. [17], it seemed implausible that these constraints were satisfied, so MSSM electroweak baryogenesis was considered unlikely. On the other hand, ref. [18] found a sizeable region of parameter space with light stops and large mass m_A for the pseudoscalar Higgs boson, in which the transition was strong enough for baryogenesis. However, a careful treatment of the LEP bounds on the Higgs mass for large m_A reduces that region significantly. Both [17] and [18] studied the one-loop effective potential perturbatively at finite temperature without resummation of higher loop contributions.

A more careful analysis of this potential, including resummation of the so-called Daisy diagrams which have an important effect, was carried out in [19] (for large m_A) and [20] (for arbitrary m_A). A small region of parameter space in which the transition is strong enough remains after imposing experimental constraints. This region corresponds to large m_A (which in turn determines a Higgs spectrum with only a light Higgs boson), small $\tan\beta$ ($\tan\beta \sim 2$), light stops compatible with experimental limits and with negligible L–R mixing, heavy gluinos, and the light Higgs barely above the LEP lower limit ($m_h > 65 \text{ GeV}$). The rest of the supersymmetric particles do not influence much the transition so that their spectrum is not constrained, although the general tendency is to prefer heavy superpartners. Even if this is a significant improvement with respect to the SM, the window for baryogenesis was clearly small.

The subject was revived recently by refs. [21, 22]. In ref. [21], the region of light masses for \tilde{t}_R was increased by taking negative values of its soft-mass squared, $m_{\tilde{t}_R}^2 < 0$. Negative values of $m_{\tilde{t}_R}^2$ are associated with the existence of dangerous colour-breaking minima in the MSSM multi-scalar potential. While in [19, 20] the lower limit on $m_{\tilde{t}_R}^2$ was set to zero, [21] shows that moderately negative values of $m_{\tilde{t}_R}^2$ can still be cosmologically allowed; the electroweak minimum is the deepest one, and is the one populated when the Universe cools down. By moving into a region with smaller $m_{\tilde{t}_R}$ (while keeping negligible mixing), the electroweak transition is stronger and sphaleron erasure can be avoided (see also [23]), thus enlarging the region where electroweak baryogenesis could take place.

In ref. [22], it was shown that two-loop QCD corrections associated with light stops dramatically affect the quantitative behaviour of the effective potential. Inclusion of these contributions is then mandatory for a more precise study of the transition, and these corrections make it strong enough for baryogenesis even if $m_{\tilde{t}_R}^2 > 0$. Therefore, this effect improves the situation in all the regions of parameter space with light stops.

Both [21] and [22] focused on the large m_A –small $\tan\beta$ region of parameter space preferred for baryogenesis and used perturbative calculations of the temperature dependent effective

potential. As discussed in [21, 22, 24], the perturbative treatment is expected to give reliable results for Higgs masses larger than in the SM case (where the limit for the validity of perturbative calculations was roughly around m_W). A very useful complementary approach was followed in refs. [25, 26, 27], where 3d effective theories [28, 29] were constructed to study the high temperature phase of the MSSM and, in particular, the nature of the electroweak transition. For not too small m_U^2 , the relevant 3d effective theory is well approximated by an $SU(2) + \text{Higgs}$ model (as in the SM but with different couplings) for which there exist non-perturbative lattice studies. The results of these analyses are in reasonable agreement³ with those of [21, 22]. A region with a strong transition is confirmed for light stops (in particular light \tilde{t}_R), small stop mixing, small $\tan\beta$, and Higgs masses up to about 80 GeV.

In any case, it is important to keep in mind that for small values of m_U (the interesting region for baryogenesis) the relevant 3d effective theory is no longer $SU(2) + \text{Higgs}$, but \tilde{t}_R and gluons should also be taken into account. The construction of such an effective theory is straightforward and was sketched in [25], but Monte Carlo simulations for that theory are not available. Another possible shortcoming of the existent 3d reduction studies may show up in the small m_A region where the two Higgs doublets are light. In such a case the effective theory may require the presence of both Higgses; it may not be justifiable to integrate out the heavier of the two. This point is discussed in more detail in the next sections.

The purpose of this paper is to further continue the perturbative exploration of the MSSM baryogenesis window in the region of small and moderate m_A , including the important two-loop corrections. As we will show, smaller m_A always corresponds to a weakening of the transition so that (for fixed values of other parameters) there is a lower bound on m_A below which the transition is too weak for baryogenesis. This lower limit decreases for smaller $\tan\beta$.

The small m_A case is interesting for several reasons. First, it can be preferred in some mechanism for the generation of baryon number [7]. Second, in the case of small m_A -large $\tan\beta$, the spontaneous CP violation mechanism of ref. [14] already mentioned could play an important rôle in baryogenesis. Unfortunately, we do not find any allowed region for large values of $\tan\beta$. Finally, the 3d approach in this region may be less straightforward than for large m_A . In particular, contact with the Monte Carlo lattice results for the $SU(2)+ \text{Higgs}$ theory could be hampered by the necessity of keeping both Higgses in the effective theory.

In this paper we are going to make a purely perturbative analysis of the transition, so we take some time to discuss in section 2 the range of parameter space where non-perturbative effects start to play a non-negligible rôle in the phase transition. In analogy with the SM case, we expect that this range is associated with the change in the nature of the EWPHT from first order to a crossover. We discuss in section 3 the expectations for a strong phase transition in the $(m_A, \tan\beta)$ parameter space making a simple qualitative analysis of the effective potential, both at zero temperature and including the dominant temperature corrections. In section 4, we write the high temperature effective potential at one-loop order with Daisy resummation, concentrating on the small m_A region. In section 5,

³ Some of the results obtained in [27] were artifacts of an implicit expansion in the stop mixing over the Debye masses and disappear when the convergence of this expansion is under control [30]. In particular, the baryogenesis region of small m_A -large $\tan\beta$ found in [27] does not subsist.

we consider the effect of dominant contributions to the two-loop resummed potential. We present our results in section 6 and our conclusions in section 7. In appendix A, we collect field dependent masses and mixing angles (both at zero and finite T) for the particles relevant to our study. Appendix B gives the lengthy expression for the non-expanded full two-loop potential. Finally, appendix C contains the dominant contributions to the two-loop resummed potential in a high T expansion.

2 Crossover in the MSSM

In the MSSM with light stops, the expansion parameter of the resummed perturbation theory at finite temperature is $\epsilon_{MSSM} \sim h_t^2/\lambda$ rather than $\epsilon_{SM} \sim g^2/\lambda$ [21, 22, 24], where h_t is the top Yukawa coupling, g the $SU(2)_L$ gauge coupling and λ the quartic Higgs boson coupling. Perturbation theory is expected to be applicable to the study of the EWPHT in the MSSM for a range of Higgs masses wider than in the SM, with a critical upper limit governed by m_t instead of m_W . We present a rough estimate of a related quantity, the critical Higgs mass beyond which the phase transition changes from first-order to a crossover. In the SM, it is possible to estimate this mass analytically by imposing the equality of the transverse W mass in the broken and symmetric phases at the critical temperature [31]. The argument arises naturally in the context of the 3d reduced theory but we use 4d quantities in what follows. The mass in the broken phase is given by

$$m_W(T_c)_{br} = \frac{1}{2}gv(T_c), \quad (2)$$

where the vev $v(T_c)$ can be obtained from the effective potential

$$V \simeq \frac{1}{2}m^2(T)\varphi^2 + \frac{1}{8}\lambda(T)\varphi^4 - \frac{T}{16\pi}g^3\varphi^3. \quad (3)$$

The mass in the symmetric phase, the magnetic mass, is of non-perturbative origin and can be estimated by solving a set of gap equations [32, 33]. It is

$$m_W(T_c)_{sym} = Cg^2T_c, \quad (4)$$

where $C = 0.28$ in the Standard Model [33] (it is basically equal to its value in the $SU(2)$ - σ model). Equating (2) and (4) and solving for λ one arrives at the critical mass for the onset of crossover

$$m_h^c = \sqrt{\frac{3}{4\pi C}}m_W \sim 74 \text{ GeV} . \quad (5)$$

This naive estimate is close to the numerical result of lattice simulations [34] which give $m_h^c \sim 80 \text{ GeV}$.

In the MSSM case with large m_A and light stops, we add to the potential (3) the stop contribution, roughly approximated by

$$\delta V \simeq -r\frac{T}{4\pi\sqrt{2}}h_{t,SM}^3\varphi^3, \quad (6)$$

where $h_{t,SM} = h_t \sin \beta$, and the constant r parameterizes the effective strength of the stop corrections. It is normalized in such a way that it would be equal to 1 if all screening effects from soft and thermal masses were negligible. In realistic cases $r \ll 1$. Heavy soft masses or light gluinos (which give a sizeable contribution to the stop thermal mass) would decrease r . On the other hand, a negative value for m_U^2 tends to increase r . From the numerical study of the transition, we can estimate that $r \sim 0.2$ when stops affect the transition sizeably without conflicting with experimental constraints.

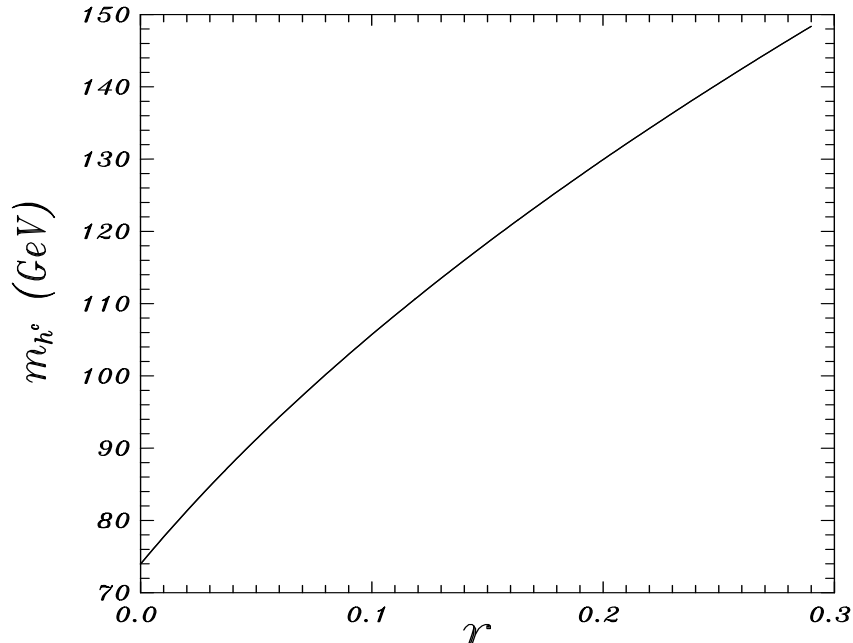


Figure 1: Critical Higgs boson mass for crossover in the MSSM [as estimated by formula (7)]. The parameter r measures the effect of stops on the transition: $r = 0$ corresponds to the pure SM limit and realistic values of r should not be larger than 0.2 – 0.3.

The magnetic mass does not depend on the presence of stops (in the same way that it is not sensitive to the Higgs mass in the SM) and it should be well approximated by the same expression (4). The following estimate for m_h^c in the MSSM follows

$$m_h^c = m_W \sqrt{\frac{3}{4\pi C} \left(1 + r \frac{m_t^3}{m_W^3} \right)}. \quad (7)$$

Eq. (7) is plotted as a function of the parameter r in figure 1. Due to the m_t^3 factor, m_h^c grows very rapidly with r ; for example, $r \sim 0.1$ corresponds to $m_h^c \sim 100 \text{ GeV}$. Below the curve the electroweak phase transition is first-order, and weakens as the curve is approached. Above the line there is not a phase transition, but an analytic crossover.

To interpret figure 1 correctly one needs to take into account that a change in the masses of the stops affects r directly, and m_h through radiative corrections. Moreover, we have obtained eq. (7) for the case of large m_A , when λ in (3) can be directly related to the light Higgs boson mass. For lower m_A one can still obtain a critical value λ^c for λ , but its relation to m_h^c involves the mixing angle between the two Higgs scalars (and $m_h^c \leq \lambda^c v$). An alternative way to describe the emergence of crossover is to equate (2) and (4) to obtain $v/T_c \sim 2Cg \sim 0.4$, and interpret this as the critical value for the jump in the order parameter as computed in perturbation theory. When perturbatively the transition is so weak, non-perturbative effects can no longer be neglected and they would eventually change the transition from first order to a crossover.

3 Parameter Space

Light stops increase the strength of the electroweak phase transition in the MSSM. Whether this effect is large enough to permit baryogenesis depends on the details of the Higgs sector at $T = 0$. At tree-level, this sector is completely determined by two parameters: the pseudoscalar mass m_A , and $\tan\beta$, the ratio of Higgs vevs at zero T . In this section we explore the plane $(m_A, \tan\beta)$ showing the expectations for a strong phase transition.

1) Large m_A ($m_A \gg m_Z, T_c$).

In this case only one Higgs doublet remains at the electroweak scale and is related to symmetry breaking, while the other is heavy and decouples from the problem. The Higgs potential relevant to the study of the electroweak transition is SM-like, $V(\varphi)$, with $\varphi = \varphi_1 \cos\beta + \varphi_2 \sin\beta$, but the light Higgs mass is not a free parameter as in the SM and it is determined at one-loop [35] to be

$$m_h^2 = m_Z^2 \cos^2 2\beta + \frac{3}{2\pi^2} \frac{m_t^4}{v^2} \log \frac{m_{\tilde{t}_1} m_{\tilde{t}_2}}{m_t^2} + f(A_t + \mu/\tan\beta). \quad (8)$$

The logarithmic radiative correction increases with increasing stop masses and can be sizeable. The last term in (8) depends on the stop mixing through the combination $X_t = A_t + \mu/\tan\beta$ and reads:

$$f(X_t) = \frac{3}{4\pi^2} \frac{m_t^4}{v^2} X_t^2 \left[2h(m_{\tilde{t}_1}^2, m_{\tilde{t}_2}^2) + X_t^2 f(m_{\tilde{t}_1}^2, m_{\tilde{t}_2}^2) \right], \quad (9)$$

where

$$h(a, b) = \frac{1}{a-b} \log \frac{a}{b}, \quad (10)$$

and

$$g(a, b) = \frac{1}{(a-b)^2} \left[2 - \frac{a+b}{a-b} \log \frac{a}{b} \right]. \quad (11)$$

The correction (9) is zero if the stop mixing is negligible ("zero mixing" case), reaches a positive maximum for large values of the mixing ("maximal mixing" case), then drops (even getting negative) if the mixing is further increased ("extreme mixing" case).

As in the SM case, the phase transition becomes weaker for larger m_h , so the best region for baryogenesis always corresponds to a region with lightest possible Higgs mass⁴. From (8), we see that the region preferred to get a strong transition is one with small $\tan\beta$, and light stops with negligible mixing (the case of a light Higgs due to extreme mixing will be discussed later). Of course, it is not enough to have a light Higgs if no effect beyond the SM helps to strengthen the transition. There are two benefits of having light stops; first, the radiative corrections to the Higgs mass are smaller for lighter stops so that the Higgs boson can be lighter. Second, direct stop contributions to the $T \neq 0$ potential enhance the transition strength (for small mixing). These ingredients describe the well known region preferred for baryogenesis. We now examine other possible effects to see if we can find additional regions supporting a strong phase transition.

- *Intermediate mass stops*

If the stops are very heavy compared to the transition temperature, their thermal contributions are Boltzmann suppressed and the SM case for the corresponding m_h is recovered. On the other hand, moderately heavy stops can still influence the transition via a $T = 0$ effect described in [36] (see also the discussion in [17]). If we neglect all couplings other than h_t in the loop corrections, the one-loop $T = 0$ potential can be written approximately as

$$V(\varphi) = -\frac{1}{2}m^2\varphi^2 + \frac{1}{4}\lambda\varphi^4 + \frac{6}{64\pi^2} \left[m_{\bar{t}_1}^4 \left(\log \frac{m_{\bar{t}_1}^2}{Q^2} - \frac{3}{2} \right) + m_{\bar{t}_2}^4 \left(\log \frac{m_{\bar{t}_2}^2}{Q^2} - \frac{3}{2} \right) - 2m_t^4 \left(\log \frac{m_t^2}{Q^2} - \frac{3}{2} \right) \right], \quad (12)$$

where $m_{\bar{t}_{1,2}}$ and m_t are field-dependent quantities and can be found in appendix A (making the replacement $\varphi_1 \rightarrow \varphi \cos\beta$, $\varphi_2 \rightarrow \varphi \sin\beta$, appropriate in the large m_A limit). When stops are heavy (for example, with equal soft masses $m_Q = m_U \equiv M_S$) compared to m_t , it is possible to expand their contribution to the potential in powers of φ/M_S . If we express m^2 and λ of eq. (12) in terms of the radiatively corrected vev v and mass m_h , the potential takes the simple form

$$V(\varphi) = \frac{1}{4}\varphi^2(\varphi^2 - v^2)\frac{m_h^2}{v^2} + \Delta V_t(\varphi) + \Delta V_{\bar{t}}(\varphi), \quad (13)$$

with

$$\Delta V_t(\varphi) = -\frac{m_t^4}{\pi^2} \frac{\varphi^2}{v^2} \left[1 + \frac{\varphi^2}{v^2} \left(\log \frac{\varphi^2}{v^2} - \frac{3}{2} \right) \right], \quad (14)$$

and

$$\Delta V_{\bar{t}}(\varphi) = \kappa \frac{m_t^4}{\pi^2} \frac{\varphi^2}{M_S^2} \left(3 - 6\frac{\varphi^2}{v^4} + 4\frac{\varphi^4}{v^4} \right) + \mathcal{O}(\varphi^8/M_S^4). \quad (15)$$

⁴The fact that the light Higgs is SM-like implies that the usual LEP bound on its mass ($m_h > 65 \text{ GeV}$) also applies; for large m_A there is no possibility of accessing lower values of m_h to strengthen the transition.

Here

$$\kappa = 1 - \frac{3X_t^2}{2M_S^2}. \quad (16)$$

$\Delta V_{\tilde{t},\tilde{t}}(\varphi)$ satisfy $\Delta V' = \Delta V'' = 0$ at $\varphi = v$ so that they do not affect v or m_h . Although $\Delta V_{\tilde{t}}$ shows the decoupling explicitly, it represents a deviation from the pure SM potential for not so large values of M_S . This effect corrects the transition strength for a fixed Higgs mass. For example, if $M_S = 500 \text{ GeV}$ the increase in $v(T_c)/T_c$ with respect to the SM with the same Higgs mass can be estimated to be a factor $1 + 0.1\kappa$ larger. This is a 10% effect if the stop mixing is negligible. Unfortunately, this modest increase for heavy stops is counterbalanced by the direct increase of m_h through radiative corrections so there is no net gain, and larger stop masses always give a weaker transition. On the other hand, it is apparent from (16) that stop mixing tends to weaken the enhancement of $v(T_c)/T_c$, eventually having a negative effect⁵.

- *Extreme stop mixing*

In this case, one may hope to get small masses for the Higgs boson via a negative radiative correction from the last term in (8). To reach this region either one or both stops should be heavy, otherwise the large mixing would drive the lighter stop mass to an imaginary value. When both stops are heavy, the situation is described by the preceding paragraph. If one stop remains light (say \tilde{t}_R , to avoid problems with $\Delta\rho$), its mass squared takes the form

$$m_{\tilde{t}_1}^2 = m_U^2 + \frac{1}{2}h_t^2 \sin^2 \beta \varphi^2 \left(1 - \frac{X_t^2}{m_Q^2}\right) + D_R(\varphi), \quad (17)$$

in which $D_R(\varphi)$ is the D term contribution, and m_U (m_Q) is the \tilde{t}_R (\tilde{t}_L) soft mass. Eq. (17) shows that the coupling to the Higgs field φ is reduced by the mixing, and the influence of this stop on the transition diminishes [21]. Thus, no improvement is expected over the SM in this region.

- *Stop mixing two-loop effects*

These corrections, calculated in [22], can have two different effects. First, the stop mixing angle α_t appears in the stop contributions. This changes the corrections slightly but no dramatic enhancement appears. The second effect, potentially more important, arises from a set of corrections that depend on the new trilinear coupling $h - \tilde{t} - \tilde{t}$. The dominant contribution of setting sun diagrams involving this coupling is [22]:

$$\begin{aligned} \delta V = & \frac{N_c T^2}{16\pi^2} (h_t \sin \beta X_t)^2 \left[\log \frac{\overline{m}_h + \overline{m}_{\tilde{t}_1} + \overline{m}_{\tilde{t}_2}}{3T} + \log \frac{\overline{m}_G + \overline{m}_{\tilde{t}_1} + \overline{m}_{\tilde{t}_2}}{3T} \right. \\ & \left. + \log \frac{\overline{m}_G + \overline{m}_{\tilde{t}_1} + \overline{m}_{\tilde{b}_L}}{3T} + \log \frac{\overline{m}_G + \overline{m}_{\tilde{t}_1} + \overline{m}_{\tilde{b}_L}}{3T} \right]. \end{aligned} \quad (18)$$

⁵The rest of squarks and sleptons give only a small correction (see [17]) through this effect. On the other hand, if they are lighter and in thermal equilibrium they raise the screening masses of stops and thus have a negative effect on the transition strength (see however [26]).

Barred scalar masses in this expression include effects from thermal screening. We have omitted in (18) other contributions proportional to gauge couplings or h_b , as well as terms of the type $\log[(m_h + 2m_{\tilde{t}_1})/(m_h + 2m_{\tilde{t}_2})]$, that have a small effect on v/T_c (a more refined approximation can be obtained from ref. [22]).

It is a simple exercise to show that a contribution to the potential of the form $\delta V = K \log[(\varphi^2 + \Pi)/\Pi]$ increases v/T_c for positive K (see [37]). The contribution (18), which can be approximated by an expression of this form, tends then to raise v/T_c . However, keeping in mind that X_t cannot be made much larger than the scale T , rough numerical estimates show that this two-loop enhancement of v/T_c is below the few percent level, while the negative effect of a non zero X_t at one-loop level [19] is quite significant.

2) Small m_A ($m_A \sim m_Z, T_c$).

For low m_A the transition is not forced to proceed along the fixed direction $\varphi_2/\varphi_1 = \tan \beta$. Consider the ($T \neq 0$) mass matrix at the origin $\varphi_1 = \varphi_2 = 0$ and define the field-direction of the lowest eigenvalue as $\varphi = \varphi_1 \cos \theta(T) + \varphi_2 \sin \theta(T)$. The behaviour of $\theta(T)$ has been studied in refs. [20, 26]. At $T = 0$ it is given by

$$\tan 2\theta \simeq \frac{m_A^2 \tan 2\beta}{m_A^2 + M_Z^2 + \Delta m^2 / \cos 2\beta}, \quad (19)$$

where $\Delta m^2 > 0$ is a one-loop correction term that can be found in [20]. We see that $\tan \theta \geq \tan \beta$ and for sufficiently low m_A , $\tan \theta \gg \tan \beta$. When T increases, the radiative corrections in (19) receive a negative contribution that grows like $h_t^2 T^2$, which decreases $\tan \theta(T)$. The critical temperature for the transition is usually reached for $\tan \theta(T_c) \gg \tan \beta$ (see [20]).⁶

In the low m_A -low $\tan \beta$ (~ 1) region, $\theta(T_c)$ could be below $\tan \beta$ [26]. In general, $\tan \theta(T_c)$ is approximately equal to $\varphi_2(T_c)/\varphi_1(T_c)$ [20] with the larger differences being expected for low $\tan \beta$. If $\tan \theta(T_c)$ and $\varphi_2(T_c)/\varphi_1(T_c)$ differ significantly, the usual procedure of integrating out the heavy Higgs at T_c may not be justified in the construction of 3d effective theories, at least to study v/T_c . However, as already noted in [26], this discrepancy is most significant for values of m_A and $\tan \beta$ excluded experimentally. Nevertheless, it is important to keep this possible complication in mind when constructing 3d effective theories for models with a non-minimal Higgs sector.

In the most common case, $\theta(T_c) \sim \varphi_2(T_c)/\varphi_1(T_c)$, and we can safely assume that the transition takes place along that direction. In particular, we note that the Higgs quartic coupling relevant to determine the strength of the transition is the quartic self coupling of that particular direction. In other words, the Higgs mass whose magnitude controls the transition strength is some effective mass for excitations along the field direction excited in the transition⁷. In principle, this is not the mass of any of the physical Higgses. It is straightforward to obtain an expression for this effective mass which is the one written in

⁶In the language of 3d effective theories, the heavy Higgs field that can be integrated out at the moment of the transition is basically H_1 for small m_A .

⁷A similar observation is helpful to estimate rather accurately the sphaleron mass in the MSSM [38].

eq. (8) with the replacement $\beta \rightarrow \theta(T_c)$. At low m_A , the physical mass of the lightest Higgs is below (8) and the corresponding eigenstate is associated with excitations in a field direction different than $\theta(T_c)$.

If one starts with some v/T_c for large m_A and fixed $\tan \beta$, the two effects just described cooperate to decrease v/T_c as m_A lowers; lower values of m_A increase $\tan \theta(T_c)$, which probes larger effective masses and thus weakens the transition. The maximal value of (8) is already saturated for large $\tan \beta$, so $\tan \theta(T_c) \gg \tan \beta$ does not make much difference in that case: in the large $\tan \beta$ regime the transition tends to have v/T_c small and independent of $\tan \beta$. This feature is actually observed in refs. [25, 26]. The only low m_A region where one can hope for a strong transition is once again the region with low $\tan \beta$, although it is expected to be reduced with respect to the large m_A case.

The qualitative behaviour described in the previous discussions is confirmed by numerical computations of v/T_c . In the rest of the paper, we focus on the small m_A region and compute v/T_c by studying the effective potential up to two loop order in resummed perturbation theory.

4 One-loop resummed potential

In this paper, we assume that the only particles present at the energy scale of the electroweak phase transition are the SM particles plus the extra MSSM Higgs doublet and squarks of the third generation [$\tilde{Q}_L = (\tilde{t}_L, \tilde{b}_L)$ and \tilde{t}_R, \tilde{b}_R]. The masses of the rest of the supersymmetric particles are assumed to be large compared to the critical temperature of the transition and their contributions are Boltzmann-suppressed. This is just a simplifying assumption and our results are qualitatively the same for more general spectra. The most important point is that gluinos should be heavy and Boltzmann-decoupled. If not, they would give significant contributions to the thermal masses for stops [19, 20], making them heavier and weakening the phase transition. The details of the transition depend weakly on the rest of the spectrum. Our model gives a fair estimate of the phase transition strength for realistic supersymmetric spectra (in particular models with a neutral LSP), with the only condition that gluinos should be heavy.

For general values of m_A , the effective potential is a function of two Higgs background fields: $\varphi_1 = \langle H_1^0 \rangle \sqrt{2}$ and $\varphi_2 = \langle H_2^0 \rangle \sqrt{2}$, in which H_i^0 are the neutral components of the two MSSM Higgs doublets. At $T = 0$, $\varphi_2/\varphi_1 = v_2/v_1 = \tan \beta$ and $v_1^2 + v_2^2 = (246 \text{ GeV})^2$.

The tree-level effective potential is

$$V_0(\varphi_1, \varphi_2) = \frac{1}{2}m_1^2\varphi_1^2 + \frac{1}{2}m_2^2\varphi_2^2 + m_{12}^2\varphi_1\varphi_2 + \frac{g^2 + g'^2}{32}(\varphi_1^2 - \varphi_2^2)^2, \quad (20)$$

with the tree-level quartic couplings fixed by SUSY in terms of gauge couplings as shown.

At one-loop (with resummation of Daisy diagrams), the effective potential (written in

$\overline{\text{MS}}$ scheme and 't Hooft-Landau gauge) receives the contribution:

$$V_1(\varphi_1, \varphi_2) = \frac{1}{2\pi^2} \sum_i n_i \left\{ \frac{1}{32} m_i^4(\varphi_1, \varphi_2) \left[\log \frac{m_i^2(\varphi_1, \varphi_2)}{Q^2} - C_i \right] + T^4 \tilde{J}_i \left[\frac{m_i^2(\varphi_1, \varphi_2)}{T^2} \right] \right\} . \quad (21)$$

The field-dependent masses $m_i^2(\varphi_1, \varphi_2)$ for gauge bosons, top and bottom, Higgses and third generation of squarks are given in appendix A, both at zero temperature and in the thermal plasma. The n_i 's are the number of degrees of freedom and can also be found in the appendix A, Q is the renormalization scale, and $C_i = 5/6$ ($3/2$) for gauge bosons (scalars and fermions). The mass parameters $m_{1,2}^2$ can be traded by $v_{1,2}^2$ by minimizing the $T = 0$ one-loop potential [20]. The \tilde{J}_i 's give the finite temperature effects; the tilde denotes that daisy resummation has been performed in the J_i 's. Here $J_i = J_{\pm}$ is the free energy of an ideal gas of particles of mass $m_i(\varphi_1, \varphi_2)$,

$$J_{\pm}(m^2/T^2) \equiv \int_0^{\infty} dx x^2 \log \left(1 \mp e^{-\sqrt{x^2+m^2/T^2}} \right) , \quad (22)$$

where $+(-)$ is for bosons (fermions). No Daisy resummation is needed for fermions and $\tilde{J}_- = J_-$. In the scalar sector, we choose to perform this resummation not only on the zero Matsubara modes but on all of them [39], so that

$$\tilde{J}_+^{(scalar)}(m_i^2) = J_+(\overline{m}_i^2) , \quad (23)$$

where the \overline{m}_i^2 are the thermally corrected masses as given in appendix A. We perform daisy resummation for gauge bosons by screening the $n = 0$ modes of longitudinal components W_L, Z_L, γ_L, g_L :

$$\tilde{J}_+(m_{i,long}^2) = J_+(m_i^2) - \frac{\pi}{6} \frac{m_{iL}^3 - m_i^3}{T^3} , \quad (24)$$

where m_{iL} are the Debye masses (to be found in appendix A). In eq. (24) the $n = 0$ (cubic) contribution to J_+ is subtracted out and replaced by a similar term with the thermally corrected mass. Transverse modes are not screened at leading order.

This potential was studied in [20], where it was shown that the presence of light stops can influence the strength of the electroweak phase transition through their contribution to the cubic $n = 0$ terms. The final region in parameter space where $v/T_c > 1$ is determined by the interplay between two opposite effects; soft and thermal screening masses tend to decrease v/T_c by screening the pure cubic behaviour of m_i^3 , while a large Yukawa coupling tends to increase v/T_c . The numerical study of the potential shows that in some region of parameter space the cubic term from stops can dominate the electroweak phase transition.

However, the only region where this transition was strong enough for baryogenesis was limited to the large m_A , small $\tan\beta$, negligible stop mixing regime. For example, with a top quark pole mass $M_t = 156 \text{ GeV}$, stop soft masses $m_Q = 70 \text{ GeV}$, $m_U = 0$, zero stop mixing $A_t = \mu = 0$ and $\tan\beta = 2.5$ the ratio v/T_c , which is ~ 1 for large m_A , drops below 0.5 for $m_A = 50 \text{ GeV}$. This is shown in curve (b) of figure 2. Here $v = \sqrt{v_1^2 + v_2^2}$, and T_c is defined by the coexistence of two degenerate minima in the T-dependent effective potential,

one at $(\varphi_1, \varphi_2) = (0, 0)$ and the other at (v_1, v_2) . The behaviour shown in figure 2 agrees well with the qualitative discussion of the previous section. Some comments on the choice of parameters are in order. Unlike the case for large m_A , negligible stop mixing [$\sim (A_t\varphi_2 - \mu\varphi_1)$] with two Higgs background fields necessarily implies negligible A_t and μ . Small μ may be problematic phenomenologically⁸. However, as we have mentioned, the transition takes place for low values of m_A along a field direction for which φ_2/φ_1 is large. As a consequence, the effect of μ in the off-diagonal stop mixing is suppressed and its influence on the transition diminishes, which has been actually observed in [25]. In practice, larger values of μ can be accommodated without weakening the strength of the transition. We can then safely set $A_t = \mu = 0$ for the purpose of analyzing the transition strength and this simplifies considerably the analysis. In the following we refer to \tilde{t}_R and \tilde{t}_L as mass eigenstates.

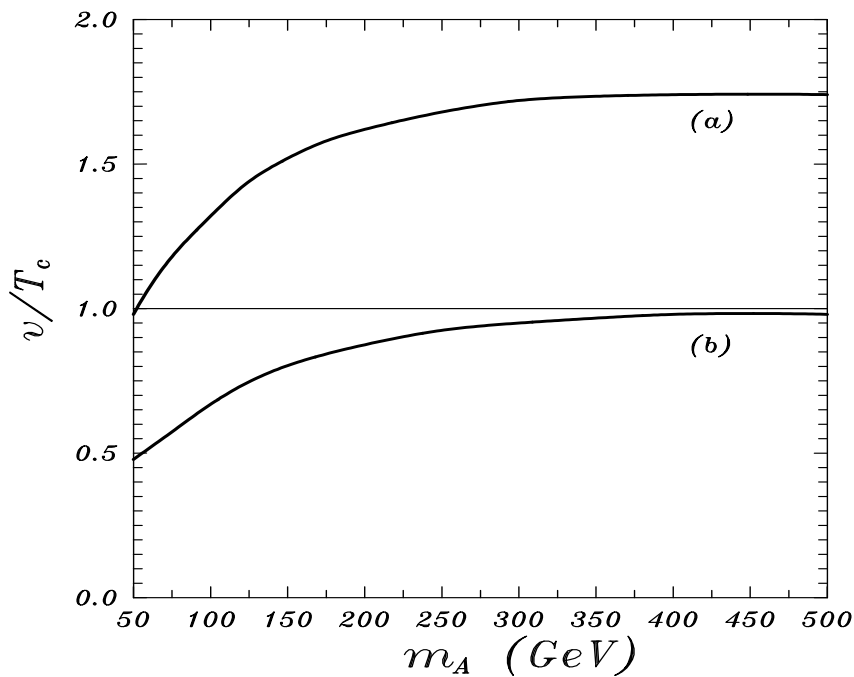


Figure 2: Order parameter v/T at T_c as a function of the pseudoscalar mass m_A . Curve (a) corresponds to the 2-loop resummed approximation, while (b) gives the 1-loop resummed result. Here $M_t = 156 \text{ GeV}$, $m_Q = 70 \text{ GeV}$, $m_U = 0$ and $\tan\beta = 2.5$.

Values of m_Q lower than 70 GeV would increase v/T_c , but they would be in conflict with $\Delta\rho$ constraints [19]. Another possibility to increase v/T_c is to choose $m_U^2 < 0$ [21]. In that case, \tilde{t}_R may get a vev and so has to be included in the discussion of the effective potential. Although, if realized, this region of parameters could have important implications (see [21, 40]) we do not explore it in this paper and we stop at $m_U = 0$. The perturbative

⁸We follow here the conventional definition of A_t and μ , which differs from the more general one used in [25].

analysis of the $T \neq 0$ potential along the squark direction (necessary to ensure that $m_U^2 < 0$ is allowed) may be problematic. We can make a rough estimate of the expansion parameter in the colour breaking minimum that may develop in the squark direction; in analogy with the SM, this expansion parameter would be the ratio of the squark quartic coupling over the $SU(3)$ gauge coupling squared. This ratio is in principle of order one. In addition, when the thermally corrected mass of \tilde{t}_R is close to zero, radiative corrections can grow very large and affect the convergence of the perturbation series along the Higgs direction. These problems have been observed in ref. [40]. Clearly a non-perturbative analysis of the $m_U^2 < 0$ region would be desirable.

However, sufficiently large values of v/T_c are obtained when two-loop corrections are taken into account [22], as we discuss in the next section, so that one is not confined to the choice $m_U^2 < 0$. In particular, this means that the condition $m_{\tilde{t}_1} < m_t$ is *not* required for a sufficiently strong phase transition.

5 Two-loop resummed potential

For simplicity, we set $g' = 0 = h_b$ in two-loop corrections. We only consider the case of negligible stop mixing, as this is the best case for a strong phase transition [20, 25].

The two-loop diagrams to consider are displayed in figure 3. Counterterm graphs are not shown. We represent Higgs bosons ($A^0, H^0, h^0, G^0, G^\pm, H^\pm$) by simple dashed lines, gauge bosons (g, W, Z, γ) by wiggly lines, squarks ($\tilde{t}_{L,R}, \tilde{b}_{L,R}$) by dashed lines with arrow, quarks (t,b) by continuous lines with arrow, and ghosts (c_W, c_Z) by dotted lines with arrow. Within the stated approximations, the full two-loop corrections to the effective potential are collected in appendix B (we follow the notation of refs. [37, 41]). In the numerical analysis we use a high temperature expansion of the different integrals, keeping terms up to order g_i^4, h_t^4 . In some corners of the parameter space we explore, for example the regions with large values of m_A and/or m_Q , this high temperature expansion starts to fail. We control our numerical results in those cases interpolating between the region where the expansion is safe and the large m_A, m_Q region where the $T \neq 0$ contributions of the heavy Higgs and/or $(\tilde{t}, \tilde{b})_L$ doublet are dropped.

The dominant two-loop terms, i.e., those that have a greater influence on the transition strength, are written down in appendix C. These are terms involving logarithms of masses. In some cases, these logarithmic terms introduce a linear dependence on the fields φ_1 and/or φ_2 for small $\varphi_{1,2}$ which is cancelled by other terms in the potential. We keep these terms to ensure that our approximation is well behaved in that respect. Finally, we also add the non-logarithmic terms which depend on the couplings g_s and h_t and thus can be potentially large (although they mainly affect the transition temperature and do not change v/T_c too much).

The relative importance of the different diagrams follows the pattern discussed in ref. [22] for the large m_A case. For low values of the stop soft masses, the main effect is due to diagram (a') with gluon exchange. This QCD contribution significantly increases the value of v/T

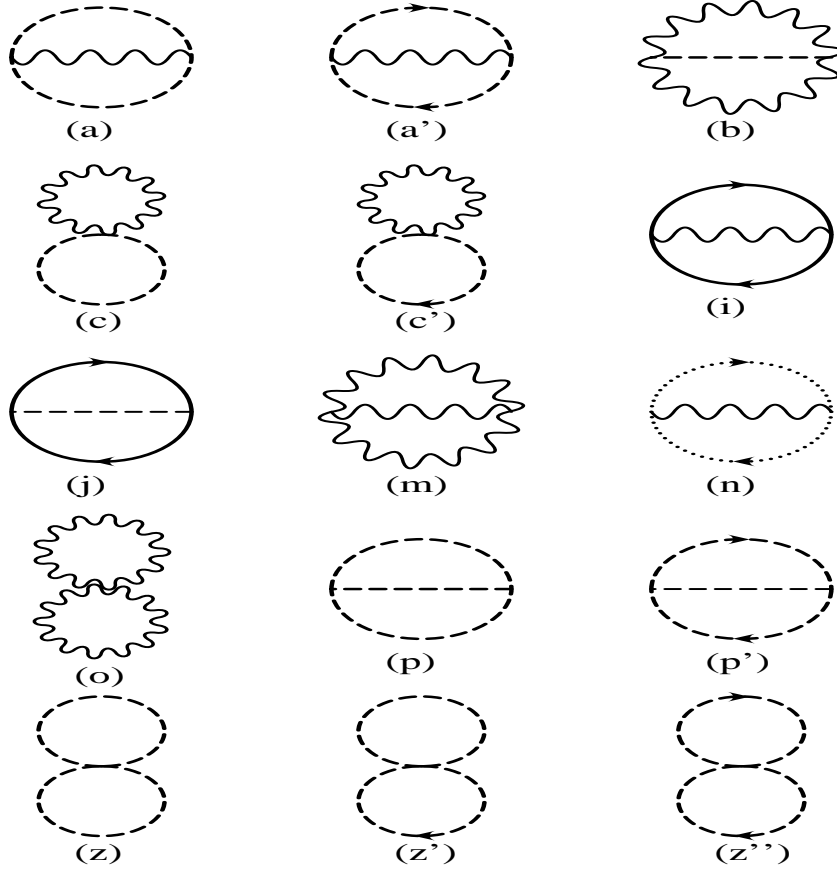


Figure 3: Two-loop vacuum graphs contributing to the effective potential (in Landau gauge). Dashed lines represent Higgs bosons, wiggled lines gauge bosons, dotted lines ghosts. Dashed lines with an arrow represent squarks, while quarks are solid lines with an arrow.

at the transition. This important enhancement is operative also in the low m_A regime as shown in fig. 2. Curve (a) gives v/T_c computed from the two-loop resummed potential as a function of the pseudoscalar mass m_A . The corresponding one-loop result is given by curve (b). The parameters have been chosen to maximize the effect.

6 Results

Before presenting the results of our numerical computation of the transition strength some comments on our definition of v/T_c are in order. We have taken T_c as the temperature of degeneracy between the symmetric and broken-phase minima. A possible alternative is to choose the temperature T_0 at which the symmetric minimum gets destabilized (that is, $V''(0) = 0$ along some field direction); in that case, the necessary condition for baryogenesis is $v/T_0 \gtrsim 1.2 - 1.3$. One can refine the precise number entering this condition by estimating

the sphaleron energy [20, 38]. The true critical temperature should be in the narrow interval $[T_0, T_c]$ if the transition is first-order. When two-loop corrections are included, in particular those of the form $\delta V \sim T^2 \varphi^2 \log \varphi$, $V''(\varphi = 0)$ diverges. This behaviour is associated with the (non-screened) transverse modes of gauge bosons. In principle, this prevents the computation of T_0 . For practical purposes, one can overcome this difficulty by turning on a small magnetic mass (which, after all, is generated non-perturbatively⁹) and checking that T_0 is not sensitive to its particular value. Although we have chosen to work with T_c , which can be defined in a cleaner way, we checked that the results obtained for v/T_0 are consistent with those that we present now.

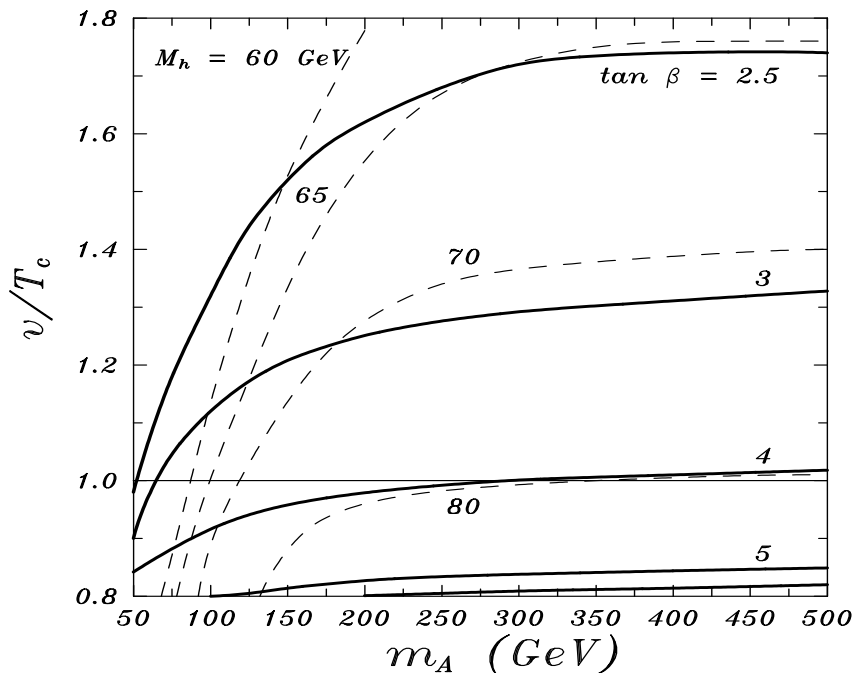


Figure 4: Lines of v/T_c (solid) for different values of $\tan \beta$ as a function of m_A . The mass of the lightest CP -even Higgs is given by the dashed contour lines. $M_t = 156 \text{ GeV}$, $m_U = 0$, $m_Q = 70 \text{ GeV}$.

In figure 4 we plot v/T_c (solid lines) as a function of the pseudoscalar mass m_A for different values of $\tan \beta$. The other relevant parameters are $M_t = 156 \text{ GeV}$ (a low value that roughly corresponds to the maximal effect of two-loop corrections), $m_U = 0$, and $m_Q = 70 \text{ GeV}$ (to satisfy the $\Delta\rho$ constraint). In figure 5 we repeat the plot for $M_t = 175 \text{ GeV}$ ($m_U = 0$, $m_Q = 250 \text{ GeV}$). These plots show that the transition is always stronger for lower values of $\tan \beta$ and larger values of m_A . At large m_A , v/T_c gets stabilized and the results of ref. [22] are recovered. At low m_A , v/T_c drops and the curves for different values of $\tan \beta$ get focused in a narrow range. This behaviour, previously observed in refs. [25, 26], has been discussed

⁹In the abelian-Higgs model no such magnetic mass is generated, even non-perturbatively. However, the diagrams responsible for the divergence are also absent as was to be expected.

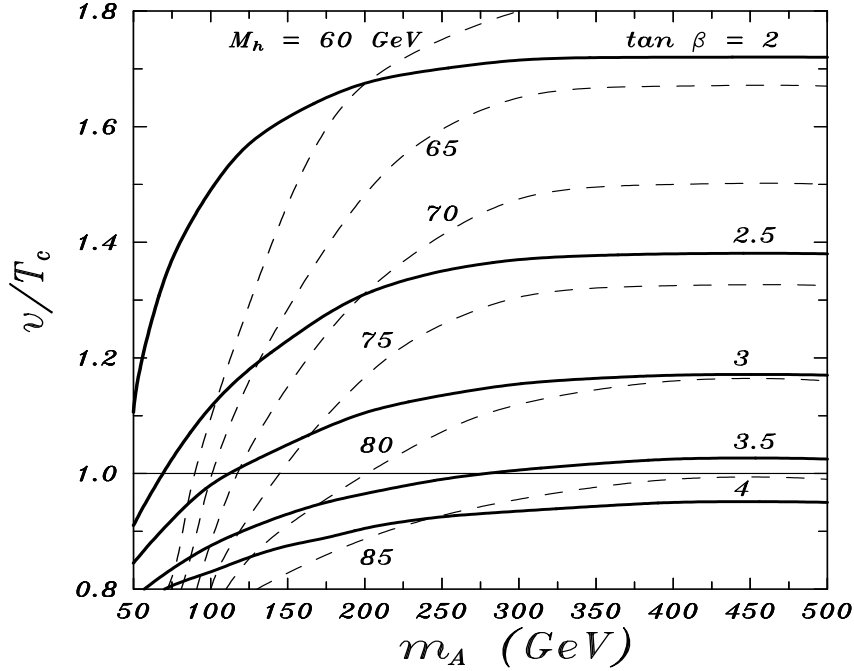


Figure 5: Same as fig. 4 but for $M_t = 175 \text{ GeV}$, $m_U = 0$, $m_Q = 250 \text{ GeV}$.

in section 3. For a given value of $\tan\beta$, there is a critical value of m_A below which the transition is too weak for baryogenesis. This critical value of m_A increases with increasing $\tan\beta$ and goes to infinity for $\tan\beta \sim 3.5 - 4$. For larger $\tan\beta$ the transition is too weak for any value of m_A .

Small $\tan\beta$ values (< 2) give a very strong transition because the Higgs mass m_h is small. Dashed lines are contour lines for m_h . In the way we are plotting our results, these curves are determined by the solid ones, because m_h depends on m_A and $\tan\beta$. We use the LEP limits on m_h to determine the experimentally allowed region. For large m_A , these limits arise from the non-observation of the production process $Z \rightarrow h^0 Z^*$, and we take the Standard Model lower limit $m_{h^0} > 65 \text{ GeV}$, because in that regime h^0 has SM couplings. For light A^0 , the process $Z \rightarrow h^0 A^0$ becomes important and in fact sets the strongest limit in the low m_A -large $\tan\beta$ region. However, that region already corresponds to $v/T_c < 1$. For our purposes, we can take the line of $m_{h^0} = 65 \text{ GeV}$ as the limit of the allowed region (it gets a few GeV weaker when $m_A \sim 100 \text{ GeV}$). After imposing the LEP bound we find from fig. 5 an absolute lower bound on m_A of about 100 GeV (below which the transition is too weak for baryogenesis) which corresponds to $\tan\beta \sim 3$. This lower bound grows for larger $\tan\beta$. The upper limit on $\tan\beta$ is $\tan\beta \lesssim 4$ and the lower limit is $\tan\beta \gtrsim 2$. The Higgs mass is below M_W , within the reach of LEP II. We find no trace of a good region for baryogenesis at low m_A and large $\tan\beta$.

Our results are in good agreement with those obtained in ref. [25] using a 3d reduced

effective theory and lattice Monte Carlo results. The upper bound on m_h of about 70 GeV quoted in that paper is smaller than our bound of 80 GeV because of the choice $m_U = 100 \text{ GeV}$ in [25]. Smaller values of m_U would allow for larger Higgs masses, as is shown in figure 5 of that paper, but in that region the approximations used to construct the reduced 3d theory start to break down. The same comments apply to the lower bound on m_A of $m_A \gtrsim 200 \text{ GeV}$, which can be lowered for smaller values of m_U .

An independent 3d analysis of the transition has been carried out in refs. [26]. It is more difficult to compare our results to theirs because they imposed SUGRA-type constraints on the parameters of the model. Of course, this restriction leads to stronger bounds on m_h , m_A and $\tan\beta$ but the qualitative dependence of the transition strength on different parameters is similar to our results.

7 Conclusion

In this paper, we have studied the electroweak phase transition in the MSSM, searching for regions where it is strong enough to permit electroweak baryogenesis. If stops are only moderately heavy they control the strength of the transition and the use of perturbation theory for its study is well justified. We first addressed the question of whether the electroweak phase transition can be a crossover in the MSSM. We clarified the differences with respect to the Standard Model case and found the critical Higgs mass for crossover, which depends on how stops affect the transition. This critical Higgs mass (beyond which the analytic crossover can take place) can be significantly larger than in the Standard Model.

We scanned the parameter space $(m_A, \tan\beta)$, qualitatively explaining the influence on the transition strength expected from different effects. We identified a region with light (unmixed) stops, light m_h , and small $\tan\beta$ where the transition can be strong. That region is widest for large m_A , and shrinks when m_A is lowered. We then focused on the interesting low m_A region and performed a numerical study evaluating the T -dependent effective potential of the model (simplified to a two Higgs doublet model plus third generation squarks) up to two-loop resummed contributions. We found that the region where the transition is strong extends down to $m_A \sim 100 \text{ GeV}$ with $2 \lesssim \tan\beta \lesssim 4$ and $m_h \lesssim 80 \text{ GeV}$ (light stops are required but $m_{\tilde{t}} < m_t$ is *not* a necessary condition). This region will be explored by LEP II in the near future, which will stringently test the viability of electroweak baryogenesis in the MSSM.

Acknowledgements

We thank J. Cline and K. Kainulainen for kindly providing us with some of the data for the analysis of ref. [27]. We also thank L. Everett for useful suggestions. B. de C. thanks the Physics and Astronomy Dept. of the University of Pennsylvania and J.R.E. thanks the Centre for Theoretical Physics of the University of Sussex for hospitality during some stages of this work, which was supported by PPARC (B. de C.) and the U.S. Department of Energy Grant No. DOE-EY-76-02-3071 (J.R.E.).

A Field-dependent Masses and Mixing Angles

We give here the field-dependent masses (in the background $\varphi_{1,2} = \langle H_{1,2}^0 \rangle \sqrt{2}$) of different species of particles relevant for the effective potential. Where appropriate, field-dependent mixing angles are defined. We also give the leading parts of thermal masses, needed for resummation of the potential. These masses are computed [42] assuming that the plasma is populated by SM particles, an extra Higgs doublet and squarks of the third generation.

- Gauge bosons:

The number of degrees of freedom is $n_W = 6$ (with $n_{W_L} = 2, n_{W_T} = 4$) and $n_{Z,\gamma} = 3$ ($n_{Z_L,\gamma_L} = 1, n_{Z_T,\gamma_T} = 2$). The masses are

$$M_W^2 = \frac{1}{4}g^2(\varphi_1^2 + \varphi_2^2), \quad M_{W_{3-B}}^2 = \frac{1}{4} \begin{pmatrix} g^2 & -gg' \\ -gg' & g'^2 \end{pmatrix} (\varphi_1^2 + \varphi_2^2), \quad (\text{A.1})$$

which gives

$$M_Z^2 = \frac{1}{4}G^2(\varphi_1^2 + \varphi_2^2), \quad M_\gamma^2 = 0, \quad (\text{A.2})$$

where $G^2 = g^2 + g'^2$.

At finite temperature the leading contribution to the thermal mass is zero (at leading order gT and to all orders in perturbation theory) for transverse modes while for longitudinal modes the above expressions change to

$$\begin{aligned} M_{W_L}^2 &\equiv M_W^2 + \Pi_{W_L} = M_W^2 + \frac{5}{2}g^2T^2, \\ M_{(W_{3-B})_L}^2 &\equiv M_{W_{3-B}}^2 + \begin{pmatrix} \Pi_{W_L} & 0 \\ 0 & \Pi_{B_L} \end{pmatrix}, \end{aligned} \quad (\text{A.3})$$

with $\Pi_{B_L} = \frac{47}{18}g'^2T^2$. The eigenvalues of $M_{(W_{3-B})_L}^2$ are $M_{Z_L}^2$ and $M_{\gamma_L}^2$. In the approximation $g' = 0$ (used for the two-loop corrections in this paper) it follows that $M_{\gamma_L} = 0$ and $M_{Z_L} = M_{W_L} \equiv M_L$.

For gluons ($n_g = 3 \times 8$) the masses are

$$M_{g_T}^2 = 0, \quad M_{g_L}^2 = 0 + \Pi_{g_L} = \frac{8}{3}g_s^2T^2. \quad (\text{A.4})$$

- Quarks:

For the third generation we have ($n_t = n_b = -12$)

$$m_t = \frac{1}{\sqrt{2}}h_t\varphi_2, \quad m_b = \frac{1}{\sqrt{2}}h_b\varphi_1. \quad (\text{A.5})$$

where h_t (h_b) is the top (bottom) Yukawa coupling.

- Squarks:

We consider only the third generation, that is, stops and sbottoms (with $n_{\tilde{t}_L} = n_{\tilde{t}_R} = n_{\tilde{b}_L} = n_{\tilde{b}_R} = 6$). The mass eigenstates are given by the diagonalization of their 2×2 mass matrix defined in terms of interaction eigenstates. For stops this is given by:

$$\begin{pmatrix} m_Q^2 + m_t^2 + \frac{1}{24}(3g^2 - g'^2)(\varphi_1^2 - \varphi_2^2) & \frac{1}{\sqrt{2}}h_t(A_t\varphi_2 + \mu\varphi_1) \\ \frac{1}{\sqrt{2}}h_t(A_t\varphi_2 + \mu\varphi_1) & m_U^2 + m_t^2 + \frac{1}{6}g'^2(\varphi_1^2 - \varphi_2^2) \end{pmatrix},$$

while for sbottoms it is:

$$\begin{pmatrix} m_Q^2 + m_b^2 - \frac{1}{24}(3g^2 + g'^2)(\varphi_1^2 - \varphi_2^2) & \frac{1}{\sqrt{2}}h_b(A_b\varphi_1 + \mu\varphi_2) \\ \frac{1}{\sqrt{2}}h_b(A_b\varphi_1 + \mu\varphi_2) & m_D^2 + m_b^2 - \frac{1}{12}g'^2(\varphi_1^2 - \varphi_2^2) \end{pmatrix}.$$

At finite T , the masses corrected by thermal effects are given (at leading order) by

$$\overline{M}_t^2 = M_t^2 + \begin{pmatrix} \Pi_Q & 0 \\ 0 & \Pi_U \end{pmatrix} ; \quad \overline{M}_b^2 = M_b^2 + \begin{pmatrix} \Pi_Q & 0 \\ 0 & \Pi_D \end{pmatrix}, \quad (\text{A.6})$$

with

$$\begin{aligned} \Pi_Q &= \frac{4}{9}g_s^2T^2 + \frac{1}{4}g^2T^2 + \frac{1}{108}g'^2T^2 + \frac{1}{6}h_t^2T^2, \\ \Pi_U &= \frac{4}{9}g_s^2T^2 + \frac{4}{27}g'^2T^2 + \frac{1}{3}h_t^2T^2, \\ \Pi_D &= \frac{4}{9}g_s^2T^2 + \frac{1}{27}g'^2T^2 + \frac{1}{3}h_t^2T^2. \end{aligned}$$

Mixing angles can be defined in the usual way. As we are interested in the case of negligible squark mixing we do not give expressions for these angles explicitly. In this case the mass and interaction eigenstates coincide.

- Higgs sector:

The two Higgs doublets are

$$\begin{pmatrix} \frac{1}{\sqrt{2}}(h_1^{0r} + \varphi_1 + ih_1^{0i}) \\ H_1^- \end{pmatrix}, \quad \begin{pmatrix} H_2^+ \\ \frac{1}{\sqrt{2}}(h_2^{0r} + \varphi_2 + ih_2^{0i}) \end{pmatrix}. \quad (\text{A.7})$$

The background $\varphi_{1,2}$ is CP conserving so that the scalar (h_1^{0r}, h_2^{0r}), pseudoscalar (h_1^{0i}, h_2^{0i}) and charged (H_1^{-*}, H_2^+) sectors can be treated separately. For each of them we have a 2×2 hermitian mass matrix

$$\mathcal{M}_{(k)}^2 = \begin{pmatrix} M_{11}^{(k)2} & M_{12}^{(k)2} \\ M_{21}^{(k)2} & M_{22}^{(k)2} \end{pmatrix}, \quad (\text{A.8})$$

(where $k = r, i, c$) and a mixing angle θ_k which relates mass eigenstates (H, h) to interaction eigenstates (H_1, H_2) according to

$$\begin{pmatrix} H_1^{(k)} \\ H_2^{(k)} \end{pmatrix} = \begin{pmatrix} \cos \theta_k & -\sin \theta_k \\ \sin \theta_k & \cos \theta_k \end{pmatrix} \begin{pmatrix} H^{(k)} \\ h^{(k)} \end{pmatrix}. \quad (\text{A.9})$$

The mixing angles are then given by:

$$\begin{aligned}\sin 2\theta_k &= \frac{2M^{(k)2}_{12}}{\sqrt{(M^{(k)2}_{11} - M^{(k)2}_{22})^2 + 4(M^{(k)2}_{12})^2}}, \\ \cos 2\theta_k &= \frac{M^{(k)2}_{11} - M^{(k)2}_{22}}{\sqrt{(M^{(k)2}_{11} - M^{(k)2}_{22})^2 + 4(M^{(k)2}_{12})^2}}.\end{aligned}\tag{A.10}$$

For the CP -even sector, $H_{1,2}^{(r)} = h_{1,2}^{0r}$, $h^{(r)} \equiv h^0$, $H^{(r)} \equiv H^0$, $n_{h^0} = n_{H^0} = 1$ and (A.8) reads:

$$\mathcal{M}_{(r)}^2 = \begin{pmatrix} m_1^2 + \frac{G^2}{8}(3\varphi_1^2 - \varphi_2^2) & m_{12}^2 - \frac{G^2}{4}\varphi_1\varphi_2 \\ m_{12}^2 - \frac{G^2}{4}\varphi_1\varphi_2 & m_2^2 + \frac{G^2}{8}(3\varphi_2^2 - \varphi_1^2) \end{pmatrix},\tag{A.11}$$

and, at finite T ,

$$\overline{\mathcal{M}}_{(r)}^2 = \mathcal{M}_{(r)}^2 + \begin{pmatrix} \Pi_1 & 0 \\ 0 & \Pi_2 \end{pmatrix},\tag{A.12}$$

with

$$\Pi_1 = \frac{1}{4}g^2T^2 + \frac{1}{12}g'^2T^2, \quad \Pi_2 = \frac{1}{4}g^2T^2 + \frac{1}{12}g'^2T^2 + \frac{3}{4}h_i^2T^2.\tag{A.13}$$

There is a mixing angle θ_r for the diagonalization of (A.11) and a T -dependent angle $\overline{\theta}_r$ for the diagonalization of (A.12).

For the CP -odd sector, $H_{1,2}^{(i)} = h_{1,2}^{0i}$, $h^{(i)} \equiv G^0$, $H^{(i)} \equiv A^0$, $n_{G^0} = n_{A^0} = 1$ and (A.8) reads:

$$\mathcal{M}_{(i)}^2 = \begin{pmatrix} m_1^2 + \frac{G^2}{8}(\varphi_1^2 - \varphi_2^2) & -m_{12}^2 \\ -m_{12}^2 & m_2^2 + \frac{G^2}{8}(\varphi_2^2 - \varphi_1^2) \end{pmatrix},\tag{A.14}$$

and, at finite T , an equation similar to (A.12) holds, with $r \rightarrow i$.

For the charged sector, $H_1^{(c)} = H_1^{-*}$, $H_2^{(c)} = H_2^+$, $h^{(c)} \equiv G^+$, $H^{(c)} \equiv H^+$, $n_{G^\pm} = n_{H^\pm} = 2$ and (A.8) reads:

$$\mathcal{M}^{(c)2} = \begin{pmatrix} m_1^2 + \frac{G^2}{8}\varphi_1^2 + \frac{(g^2-g'^2)}{8}\varphi_2^2 & -m_{12}^2 + \frac{g^2}{4}\varphi_1\varphi_2 \\ -m_{12}^2 + \frac{g^2}{4}\varphi_1\varphi_2 & m_2^2 + \frac{G^2}{8}\varphi_2^2 + \frac{(g^2-g'^2)}{8}\varphi_1^2 \end{pmatrix},\tag{A.15}$$

and, at finite T , an equation similar to (A.12) holds, with $r \rightarrow c$.

For different cross-checking purposes it is useful to consider the behaviour of the mixing angles θ_k in two different limits:

(a) In the large m_A limit

$$\theta_r \rightarrow \beta + \frac{\pi}{2}, \quad \theta_i, \theta_c \rightarrow -\beta - \frac{\pi}{2}.\tag{A.16}$$

(b) In the physical limit, $\varphi_{1,2} \rightarrow v_{1,2}$,

$$\theta_r \rightarrow \alpha, \quad \theta_i, \theta_c \rightarrow -\beta + \frac{\pi}{2},\tag{A.17}$$

where α is the physical mixing angle in the CP -even sector.

For later use it is convenient to define the following abbreviations (with the indicated limiting values $[(a), (b)]$):

$$\begin{aligned}
\varphi_0 &\equiv \varphi_1 \cos \theta_r + \varphi_2 \sin \theta_r &\rightarrow [0, v \cos(\beta - \alpha)] \\
\varphi_v &\equiv \varphi_2 \cos \theta_r - \varphi_1 \sin \theta_r &\rightarrow [\varphi, v \sin(\beta - \alpha)] \\
\varphi_{\sin} &\equiv \varphi_1 \cos \theta_r - \varphi_2 \sin \theta_r &\rightarrow [\varphi \sin 2\beta, v \cos(\beta + \alpha)] \\
\varphi_{\cos} &\equiv \varphi_2 \cos \theta_r + \varphi_1 \sin \theta_r &\rightarrow [\varphi \cos 2\beta, v \sin(\beta + \alpha)] \\
\varphi_{0,i} &\equiv \varphi_2 \sin \theta_i - \varphi_1 \cos \theta_i &\rightarrow [0, 0] \\
\varphi_{v,i} &\equiv \varphi_2 \cos \theta_i + \varphi_1 \sin \theta_i &\rightarrow [\varphi, v] \\
\varphi_{\cos,c} &\equiv \varphi_2 \cos \theta_c - \varphi_1 \sin \theta_c &\rightarrow [-\varphi \cos 2\beta, -v \cos 2\beta] \\
\varphi_{\sin,c} &\equiv \varphi_2 \sin \theta_c + \varphi_1 \cos \theta_c &\rightarrow [\varphi \sin 2\beta, v \sin 2\beta].
\end{aligned} \tag{A.18}$$

B Two-loop Resummed Potential

We present the resummed two-loop corrections to the finite temperature effective potential in the MSSM framework described in the text. We make the approximation $g' = h_b = 0$, so that in the formulae below we make no distinction between m_Z and m_W which are called M (M_L is the longitudinal component). We further assume that left-right mixing in the squark sector is small and can be neglected. We follow the notation of [37, 41] and the labeling of different contributions corresponds to our figure 3. As usual, $N_c = 3$ counts the number of colours and we use the abbreviations $c_r = \cos \theta_r$, $s_{2c} = \sin 2\theta_c$, etc. For some recurrent combinations of fields and angles (like e.g. $\varphi_1 c_r + \varphi_2 s_r$) we use the short-hand expressions defined at the end of appendix A. With our resummation method in the scalar sector (we included the thermal mass correction in all Matsubara modes) masses and mixing angles are T -dependent: $\overline{m}_i, \overline{\theta}_k$. For simplicity we drop the bars in the formulae below and simply write m_i, θ_k everywhere.

$$\begin{aligned}
V^{(a)} = & - \frac{g^2}{8} \left\{ 2 \cos^2(\theta_r + \theta_c) [\mathcal{D}_{SSV}(m_{G^\pm}, m_{h^0}, M) + \mathcal{D}_{SSV}(m_{H^\pm}, m_{H^0}, M)] \right. \\
& + 2 \sin^2(\theta_r + \theta_c) [\mathcal{D}_{SSV}(m_{G^\pm}, m_{H^0}, M) + \mathcal{D}_{SSV}(m_{H^\pm}, m_{h^0}, M)] \\
& + 2 \cos^2(\theta_c - \theta_i) [\mathcal{D}_{SSV}(m_{G^\pm}, m_{G^0}, M) + \mathcal{D}_{SSV}(m_{H^\pm}, m_{A^0}, M)] \\
& + 2 \sin^2(\theta_c - \theta_i) [\mathcal{D}_{SSV}(m_{G^\pm}, m_{A^0}, M) + \mathcal{D}_{SSV}(m_{H^\pm}, m_{G^0}, M)] \\
& + \cos^2(\theta_i + \theta_r) [\mathcal{D}_{SSV}(m_{G^0}, m_{h^0}, M) + \mathcal{D}_{SSV}(m_{A^0}, m_{H^0}, M)] \\
& + \sin^2(\theta_i + \theta_r) [\mathcal{D}_{SSV}(m_{G^0}, m_{H^0}, M) + \mathcal{D}_{SSV}(m_{h^0}, m_{A^0}, M)] \\
& \left. + \mathcal{D}_{SSV}(m_{G^\pm}, m_{G^\pm}, M) + \mathcal{D}_{SSV}(m_{H^\pm}, m_{H^\pm}, M) \right\}, \\
V^{(a')} = & - \frac{g^2}{8} N_c \left[\mathcal{D}_{SSV}(m_{\tilde{t}_L}, m_{\tilde{t}_L}, M) + \mathcal{D}_{SSV}(m_{\tilde{b}_L}, m_{\tilde{b}_L}, M) + 4 \mathcal{D}_{SSV}(m_{\tilde{t}_L}, m_{\tilde{b}_L}, M) \right] \\
& - \frac{g_s^2}{4} (N_c^2 - 1) \left[\mathcal{D}_{SSV}(m_{\tilde{t}_L}, m_{\tilde{t}_L}, 0) + \mathcal{D}_{SSV}(m_{\tilde{b}_L}, m_{\tilde{b}_L}, 0) \right]
\end{aligned}$$

$$\begin{aligned}
& + \mathcal{D}_{SSV}(m_{\tilde{t}_R}, m_{\tilde{t}_R}, 0) + \mathcal{D}_{SSV}(m_{\tilde{b}_R}, m_{\tilde{b}_R}, 0) \Big], \\
V^{(b)} = & - \frac{3}{64} g^4 \left[\varphi_v^2 \mathcal{D}_{SVV}(m_{h^0}, M, M) + \varphi_0^2 \mathcal{D}_{SVV}(m_{H^0}, M, M) \right], \\
V^{(c)} = & - \frac{3}{16} g^2 \left[2\mathcal{D}_{SV}(m_{G^\pm}, M) + \mathcal{D}_{SV}(m_{G^0}, M) + \mathcal{D}_{SV}(m_{h^0}, M) \right. \\
& + \left. 2\mathcal{D}_{SV}(m_{H^\pm}, M) + \mathcal{D}_{SV}(m_{A^0}, M) + \mathcal{D}_{SV}(m_{H^0}, M) \right], \\
V^{(c')} = & - \frac{1}{4} g_s^2 (N_c^2 - 1) \left[\mathcal{D}_{SV}(m_{\tilde{t}_L}, 0) + \mathcal{D}_{SV}(m_{\tilde{b}_L}, 0) + \mathcal{D}_{SV}(m_{\tilde{t}_R}, 0) + \mathcal{D}_{SV}(m_{\tilde{b}_R}, 0) \right] \\
& - \frac{3}{8} g^2 N_c \left[\mathcal{D}_{SV}(m_{\tilde{t}_L}, M) + \mathcal{D}_{SV}(m_{\tilde{b}_L}, M) \right], \\
V^{(i)} = & - 4g_s^2 \mathcal{D}_{ffV}(m_t, m_t, 0) - \frac{3}{8} g^2 \left[\mathcal{D}_{ffV}(m_t, m_t, M) - \mathcal{D}_{ffV}(0, 0, M) \right] \\
& - \frac{3}{2} g^2 \left[\mathcal{D}_{ffV}(m_t, 0, M) - \mathcal{D}_{ffV}(0, 0, M) \right] - 3g^2 n_t \mathcal{D}_{ffV}(0, 0, M), \\
V^{(j)} = & - \frac{N_c}{4} h_t^2 \left[c_r^2 \mathcal{D}_{ffS}(m_t, m_t, m_{h^0}) + s_r^2 \mathcal{D}_{ffS}(m_t, m_t, m_{H^0}) + c_i^2 \mathcal{D}_{ffS}(m_t, m_t, m_{G^0}) \right. \\
& + \left. s_i^2 \mathcal{D}_{ffS}(m_t, m_t, m_{A^0}) + 2c_c^2 \mathcal{D}_{ffS}(m_t, m_b, m_{G^\pm}) + 2s_c^2 \mathcal{D}_{ffS}(m_t, m_b, m_{H^\pm}) \right], \\
V^{(m)} = & - \frac{1}{2} g^2 \left[\mathcal{D}_{VVV}(M, M, M) + 3\mathcal{D}_{LLT}(M_L, M_L, M) - 3\mathcal{D}_{LLT}(M, M, M) \right], \\
V^{(n)} = & - 3g^2 \mathcal{D}_{\eta\eta V}(M), \\
V^{(o)} = & - \frac{3}{4} g^2 \mathcal{D}_{VV}(M, M), \\
V^{(p)} = & - \frac{1}{64} g^4 \left\{ 2 \left[(\varphi_v - s_{2c}\varphi_{sin})^2 \bar{\mathbb{H}}(m_{h^0}, m_{G^\pm}, m_{G^\pm}) + (\varphi_v + s_{2c}\varphi_{sin})^2 \bar{\mathbb{H}}(m_{h^0}, m_{H^\pm}, m_{H^\pm}) \right] \right. \\
& + 2 \left[(\varphi_0 - s_{2c}\varphi_{cos})^2 \bar{\mathbb{H}}(m_{H^0}, m_{G^\pm}, m_{G^\pm}) + (\varphi_0 + s_{2c}\varphi_{cos})^2 \bar{\mathbb{H}}(m_{H^0}, m_{H^\pm}, m_{H^\pm}) \right] \\
& + 4c_{2c}^2 \left[\varphi_{sin}^2 \bar{\mathbb{H}}(m_{h^0}, m_{G^\pm}, m_{H^\pm}) + \varphi_{cos}^2 \bar{\mathbb{H}}(m_{H^0}, m_{G^\pm}, m_{H^\pm}) \right] \\
& + 4 \left[\varphi_{0,i}^2 \bar{\mathbb{H}}(m_{G^0}, m_{G^\pm}, m_{H^\pm}) + \varphi_{v,i}^2 \bar{\mathbb{H}}(m_{A^0}, m_{G^\pm}, m_{H^\pm}) \right] \\
& + 3c_{2r}^2 \left[\varphi_{cos}^2 \bar{\mathbb{H}}(m_{h^0}, m_{h^0}, m_{h^0}) + \varphi_{sin}^2 \bar{\mathbb{H}}(m_{H^0}, m_{H^0}, m_{H^0}) \right] \\
& + (2\varphi_0 - 3c_{2r}\varphi_{sin})^2 \bar{\mathbb{H}}(m_{H^0}, m_{h^0}, m_{h^0}) + (2\varphi_v - 3c_{2r}\varphi_{cos})^2 \bar{\mathbb{H}}(m_{H^0}, m_{H^0}, m_{h^0}) \\
& + c_{2i}^2 \varphi_{cos}^2 \left[\bar{\mathbb{H}}(m_{h^0}, m_{G^0}, m_{G^0}) + \bar{\mathbb{H}}(m_{h^0}, m_{A^0}, m_{A^0}) \right] \\
& + c_{2i}^2 \varphi_{sin}^2 \left[\bar{\mathbb{H}}(m_{H^0}, m_{G^0}, m_{G^0}) + \bar{\mathbb{H}}(m_{H^0}, m_{A^0}, m_{A^0}) \right] \\
& + \left. 2s_{2i}^2 \left[\varphi_{cos}^2 \bar{\mathbb{H}}(m_{h^0}, m_{G^0}, m_{A^0}) + \varphi_{sin}^2 \bar{\mathbb{H}}(m_{H^0}, m_{G^0}, m_{A^0}) \right] \right\}, \\
V^{(p')} = & - \frac{1}{2} N_c \left\{ [h_t^2 c_r \varphi_2 - g^2 \varphi_{cos}/4]^2 \bar{\mathbb{H}}(m_{h^0}, m_{\tilde{t}_L}, m_{\tilde{t}_L}) + (h_t^2 c_r \varphi_2)^2 \bar{\mathbb{H}}(m_{h^0}, m_{\tilde{t}_R}, m_{\tilde{t}_R}) \right. \\
& + [h_t^2 s_r \varphi_2 + g^2 \varphi_{sin}/4]^2 \bar{\mathbb{H}}(m_{H^0}, m_{\tilde{t}_L}, m_{\tilde{t}_L}) + (h_t^2 s_r \varphi_2)^2 \bar{\mathbb{H}}(m_{H^0}, m_{\tilde{t}_R}, m_{\tilde{t}_R}) \\
& + [h_t^2 c_c \varphi_2 + g^2 \varphi_{sin,c}/2]^2 \bar{\mathbb{H}}(m_{G^\pm}, m_{\tilde{t}_L}, m_{\tilde{b}_L}) + [g^2 \varphi_{cos}/4]^2 \bar{\mathbb{H}}(m_{h^0}, m_{\tilde{b}_L}, m_{\tilde{b}_L}) \\
& + \left. [h_t^2 s_c \varphi_2 - g^2 \varphi_{cos,c}/2]^2 \bar{\mathbb{H}}(m_{H^\pm}, m_{\tilde{t}_L}, m_{\tilde{b}_L}) + [g^2 \varphi_{sin}/4]^2 \bar{\mathbb{H}}(m_{H^0}, m_{\tilde{b}_L}, m_{\tilde{b}_L}) \right\},
\end{aligned}$$

$$\begin{aligned}
V^{(z)} = & \frac{1}{16}g^2 \left\{ 4c_{2c}^2 [\mathcal{D}_S(m_{G^\pm}, m_{G^\pm}) + \mathcal{D}_S(m_{H^\pm}, m_{H^\pm})] - 4c_{4c}\mathcal{D}_S(m_{G^\pm}, m_{H^\pm}) \right. \\
& + 2[(1 + s_{2c}s_{2r}) [\mathcal{D}_S(m_{G^\pm}, m_{h^0}) + \mathcal{D}_S(m_{H^\pm}, m_{H^0})] \\
& + (1 - s_{2c}s_{2r}) [\mathcal{D}_S(m_{G^\pm}, m_{H^0}) + \mathcal{D}_S(m_{H^\pm}, m_{h^0})] \\
& + (1 - s_{2c}s_{2i}) [\mathcal{D}_S(m_{G^\pm}, m_{G^0}) + \mathcal{D}_S(m_{A^0}, m_{H^\pm})] \\
& + (1 + s_{2c}s_{2i}) [\mathcal{D}_S(m_{G^\pm}, m_{A^0}) + \mathcal{D}_S(m_{G^0}, m_{H^\pm})] \\
& + \frac{3}{2} [c_{2r}^2 [\mathcal{D}_S(m_{h^0}, m_{h^0}) + \mathcal{D}_S(m_{H^0}, m_{H^0})] + c_{2i}^2 [\mathcal{D}_S(m_{G^0}, m_{G^0}) + \mathcal{D}_S(m_{A^0}, m_{A^0})] \\
& + (2 - 3c_{2r}^2)\mathcal{D}_S(m_{h^0}, m_{H^0}) + (2 - 3c_{2i}^2)\mathcal{D}_S(m_{G^0}, m_{A^0}) \\
& + c_{2i}c_{2r} [\mathcal{D}_S(m_{h^0}, m_{G^0}) + \mathcal{D}_S(m_{H^0}, m_{A^0}) - \mathcal{D}_S(m_{h^0}, m_{A^0}) - \mathcal{D}_S(m_{H^0}, m_{G^0})] \left. \right\}, \\
V^{(z')} = & \frac{1}{2}N_c h_t^2 \left\{ c_r^2 [\mathcal{D}_S(m_{\tilde{t}_L}, m_{h^0}) + \mathcal{D}_S(m_{\tilde{t}_R}, m_{h^0})] + s_r^2 [\mathcal{D}_S(m_{\tilde{t}_L}, m_{H^0}) + \mathcal{D}_S(m_{\tilde{t}_R}, m_{H^0})] \right. \\
& + c_i^2 [\mathcal{D}_S(m_{\tilde{t}_L}, m_{G^0}) + \mathcal{D}_S(m_{\tilde{t}_R}, m_{G^0})] + s_i^2 [\mathcal{D}_S(m_{\tilde{t}_L}, m_{A^0}) + \mathcal{D}_S(m_{\tilde{t}_R}, m_{A^0})] \\
& + 2c_c^2 [\mathcal{D}_S(m_{\tilde{t}_R}, m_{G^\pm}) + \mathcal{D}_S(m_{\tilde{b}_L}, m_{G^\pm})] + 2s_c^2 [\mathcal{D}_S(m_{\tilde{t}_R}, m_{H^\pm}) + \mathcal{D}_S(m_{\tilde{b}_L}, m_{H^\pm})] \left. \right\} \\
& + \frac{1}{8}g^2 N_c \left\{ c_{2r} [\mathcal{D}_S(m_{\tilde{b}_L}, m_{h^0}) - \mathcal{D}_S(m_{\tilde{t}_L}, m_{h^0}) + \mathcal{D}_S(m_{\tilde{t}_L}, m_{H^0}) - \mathcal{D}_S(m_{\tilde{b}_L}, m_{H^0})] \right. \\
& + c_{2i} [\mathcal{D}_S(m_{\tilde{t}_L}, m_{A^0}) - \mathcal{D}_S(m_{\tilde{b}_L}, m_{A^0}) + \mathcal{D}_S(m_{\tilde{b}_L}, m_{G^0}) - \mathcal{D}_S(m_{\tilde{t}_L}, m_{G^0})] \\
& + 2c_{2c} [\mathcal{D}_S(m_{\tilde{b}_L}, m_{H^\pm}) - \mathcal{D}_S(m_{\tilde{t}_L}, m_{H^\pm}) + \mathcal{D}_S(m_{\tilde{t}_L}, m_{G^\pm}) - \mathcal{D}_S(m_{\tilde{b}_L}, m_{G^\pm})] \left. \right\}, \\
V^{(z'')} = & \frac{g^2}{4}N_c(2 - N_c)\mathcal{D}_S(m_{\tilde{t}_L}, m_{\tilde{b}_L}) + h_t^2 N_c [\mathcal{D}_S(m_{\tilde{t}_L}, m_{\tilde{t}_R}) + \mathcal{D}_S(m_{\tilde{b}_L}, m_{\tilde{t}_R})] \\
& + \left(\frac{g^2}{8} + \frac{g_s^2}{6} \right) N_c(N_c + 1) [\mathcal{D}_S(m_{\tilde{t}_L}, m_{\tilde{t}_L}) + \mathcal{D}_S(m_{\tilde{b}_L}, m_{\tilde{b}_L})] \\
& + \frac{g_s^2}{6}N_c(N_c + 1) [\mathcal{D}_S(m_{\tilde{t}_R}, m_{\tilde{t}_R}) + \mathcal{D}_S(m_{\tilde{b}_R}, m_{\tilde{b}_R})] \tag{B.1}
\end{aligned}$$

where

$$\mathcal{D}_S(m_1, m_2) = I(m_1)I(m_2).$$

In the previous formulae, dimensional regularization (with $n - 1 = 3 - 2\epsilon$) is used to evaluate divergent integrals. Poles in $1/\epsilon$ and ν_ϵ -dependent terms cancel when counterterms are included. In addition, counterterms contribute a finite piece to the potential.

With $g' = 0$ the $T = 0$ counterterm potential reads

$$\delta V_{count} = \frac{1}{2} \left\{ \frac{3}{4}(3 - 2\epsilon)I_\beta^\epsilon (\delta Z_{g^2} + \delta Z_{\varphi_1^2} + \delta Z_{\varphi_2^2}) g^2(\varphi_1^2 + \varphi_2^2) - 6h_t^2 I_{f\beta}^\epsilon (\delta Z_{h_t^2} + \delta Z_{\varphi_2^2}) \varphi_2^2 \right\},$$

with

$$I_\beta^\epsilon = \frac{T^2}{12}(1 + \epsilon\nu_\epsilon) \quad , \quad I_{f\beta}^\epsilon = -\frac{T^2}{24}[1 + \epsilon(\nu_\epsilon - \log 4)].$$

The $\overline{\text{MS}}$ renormalization functions δZ (calculated in a model with two Higgs doublets plus third generation squarks) are

$$\delta Z_{g^2} = -\frac{5}{2}g^2 \frac{1}{16\pi^2\epsilon}, \quad \delta Z_{\varphi_1^2} = \frac{9}{4}g^2 \frac{1}{16\pi^2\epsilon}, \quad \delta Z_{\varphi_2^2} = \left(\frac{9}{4}g^2 - 3h_t^2 \right) \frac{1}{16\pi^2\epsilon},$$

$$\delta Z_{h_i^2} = \left(\frac{9}{2} h_i^2 - 8g_s^2 - \frac{9}{4} g^2 \right) \frac{1}{16\pi^2 \epsilon}.$$

The finite contribution is then

$$\delta V_{count,fin} = \frac{T^2}{64\pi^2} \left[M^2(3h_i^2 - 2g^2) + m_i^2(16g_s^2 - 3h_i^2) \log 2 \right]. \quad (\text{B.2})$$

The resummation procedure we followed for scalars can be implemented by adding and subtracting the appropriate thermal mass terms for the scalars in the Lagrangian. In this way the unperturbed Lagrangian contains already thermally corrected masses and thermal counterterms appear. To cancel all divergences, diagrams involving those counterterms should be included. For the two-loop potential, one-loop thermal counterterm contributions are needed and give

$$\delta V_{th,count} = -\frac{1}{2} \sum_{i, \text{scalars}} n_i \Pi_i I(m_i^2), \quad (\text{B.3})$$

where Π_i is the thermal self-energy of the i^{th} scalar.

C High T expansion of the Potential

We give the dominant two-loop terms of the potential presented in appendix B using a high T expansion.

First we have logarithmic terms coming from bosonic setting-sun diagrams:

$$\begin{aligned} \delta V_{log}^{(a)} = & -\frac{g^2}{64\pi^2} T^2 \left\{ \cos^2(\theta_r + \theta_c) \left[\begin{aligned} & (M^2 - 2m_{G^\pm}^2 - 2m_{h^0}^2) \log \left(\frac{3T}{m_{G^\pm} + m_{h^0} + M} \right) \right. \\ & + \frac{(m_{G^\pm}^2 - m_{h^0}^2)^2}{M^2} \log \left(\frac{m_{G^\pm} + m_{h^0}}{m_{G^\pm} + m_{h^0} + M} \right) \\ & + (M^2 - 2m_{H^\pm}^2 - 2m_{H^0}^2) \log \left(\frac{3T}{m_{H^\pm} + m_{H^0} + M} \right) \\ & \left. + \frac{(m_{H^\pm}^2 - m_{H^0}^2)^2}{M^2} \log \left(\frac{m_{H^\pm} + m_{H^0}}{m_{H^\pm} + m_{H^0} + M} \right) \right] \\ & + \sin^2(\theta_r + \theta_c) \left[\begin{aligned} & (M^2 - 2m_{G^\pm}^2 - 2m_{H^0}^2) \log \left(\frac{3T}{m_{G^\pm} + m_{H^0} + M} \right) \\ & + \frac{(m_{G^\pm}^2 - m_{H^0}^2)^2}{M^2} \log \left(\frac{m_{G^\pm} + m_{H^0}}{m_{G^\pm} + m_{H^0} + M} \right) \\ & + (M^2 - 2m_{H^\pm}^2 - 2m_{h^0}^2) \log \left(\frac{3T}{m_{H^\pm} + m_{h^0} + M} \right) \\ & \left. + \frac{(m_{H^\pm}^2 - m_{h^0}^2)^2}{M^2} \log \left(\frac{m_{H^\pm} + m_{h^0}}{m_{H^\pm} + m_{h^0} + M} \right) \right] \\ & + \cos^2(\theta_c - \theta_i) \left[\begin{aligned} & (M^2 - 2m_{G^\pm}^2 - 2m_{G^0}^2) \log \left(\frac{3T}{m_{G^\pm} + m_{G^0} + M} \right) \end{aligned} \right] \end{aligned}$$

$$\begin{aligned}
& + \frac{(m_{G^\pm}^2 - m_{G^0}^2)^2}{M^2} \log \left(\frac{m_{G^\pm} + m_{G^0}}{m_{G^\pm} + m_{G^0} + M} \right) \\
& + (M^2 - 2m_{H^\pm}^2 - 2m_{A^0}^2) \log \left(\frac{3T}{m_{H^\pm} + m_{A^0} + M} \right) \\
& + \frac{(m_{H^\pm}^2 - m_{A^0}^2)^2}{M^2} \log \left(\frac{m_{H^\pm} + m_{A^0}}{m_{H^\pm} + m_{A^0} + M} \right) \quad \Big] \text{(C.1)} \\
& + \sin^2(\theta_c - \theta_i) \left[\begin{aligned}
& (M^2 - 2m_{G^\pm}^2 - 2m_{A^0}^2) \log \left(\frac{3T}{m_{G^\pm} + m_{A^0} + M} \right) \\
& + \frac{(m_{G^\pm}^2 - m_{A^0}^2)^2}{M^2} \log \left(\frac{m_{G^\pm} + m_{A^0}}{m_{G^\pm} + m_{A^0} + M} \right) \\
& + (M^2 - 2m_{H^\pm}^2 - 2m_{G^0}^2) \log \left(\frac{3T}{m_{H^\pm} + m_{G^0} + M} \right) \\
& + \frac{(m_{H^\pm}^2 - m_{G^0}^2)^2}{M^2} \log \left(\frac{m_{H^\pm} + m_{G^0}}{m_{H^\pm} + m_{G^0} + M} \right) \quad \Big] \\
& + \frac{1}{2} \cos^2(\theta_i + \theta_r) \left[\begin{aligned}
& (M^2 - 2m_{G^0}^2 - 2m_{h^0}^2) \log \left(\frac{3T}{m_{G^0} + m_{h^0} + M} \right) \\
& + \frac{(m_{G^0}^2 - m_{h^0}^2)^2}{M^2} \log \left(\frac{m_{G^0} + m_{h^0}}{m_{G^0} + m_{h^0} + M} \right) \\
& + (M^2 - 2m_{A^0}^2 - 2m_{H^0}^2) \log \left(\frac{3T}{m_{A^0} + m_{H^0} + M} \right) \\
& + \frac{(m_{A^0}^2 - m_{H^0}^2)^2}{M^2} \log \left(\frac{m_{A^0} + m_{H^0}}{m_{A^0} + m_{H^0} + M} \right) \quad \Big] \\
& + \frac{1}{2} \sin^2(\theta_i + \theta_r) \left[\begin{aligned}
& (M^2 - 2m_{G^0}^2 - 2m_{H^0}^2) \log \left(\frac{3T}{m_{G^0} + m_{H^0} + M} \right) \\
& + \frac{(m_{G^0}^2 - m_{H^0}^2)^2}{M^2} \log \left(\frac{m_{G^0} + m_{H^0}}{m_{G^0} + m_{H^0} + M} \right) \\
& + (M^2 - 2m_{A^0}^2 - 2m_{h^0}^2) \log \left(\frac{3T}{m_{A^0} + m_{h^0} + M} \right) \\
& + \frac{(m_{A^0}^2 - m_{h^0}^2)^2}{M^2} \log \left(\frac{m_{A^0} + m_{h^0}}{m_{A^0} + m_{h^0} + M} \right) \quad \Big] \\
& + \frac{1}{2} (M^2 - 4m_{G^\pm}^2) \log \left(\frac{3T}{2m_{G^\pm} + M} \right) + \frac{1}{2} (M^2 - 4m_{H^\pm}^2) \log \left(\frac{3T}{2m_{H^\pm} + M} \right) \Big\}
\end{aligned}
\end{aligned}$$

$$\begin{aligned}
\delta V_{log}^{(b)} = & -\frac{3g^4}{64\pi^2} \frac{T^2}{8} \left\{ \varphi_v^2 \left[\begin{aligned}
& \frac{m_{h^0}^4}{2M^4} \left[\log \left(\frac{m_{h^0} + M}{m_{h^0} + 2M} \right) + \log \left(\frac{m_{h^0} + M}{m_{h^0}} \right) \right] \right. \\
& + 2 \log \left(\frac{m_{h^0} + 2M}{m_{h^0} + 2M_L} \right) + 5 \log \left(\frac{3T}{m_{h^0} + 2M} \right) + \frac{M^2 - 2m_{h^0}^2}{M^2} \log \left(\frac{m_{h^0} + M}{m_{h^0} + 2M} \right) \quad \Big] \\
& + \varphi_0^2 \left[\begin{aligned}
& \frac{m_{H^0}^4}{2M^4} \left[\log \left(\frac{m_{H^0} + M}{m_{H^0} + 2M} \right) + \log \left(\frac{m_{H^0} + M}{m_{H^0}} \right) \right] \quad \Big] \quad \text{(C.2)}
\end{aligned}
\end{aligned}
\right.
\end{aligned}$$

$$\begin{aligned}
& \left. + 2 \log \left(\frac{m_{H^0} + 2M}{m_{H^0} + 2M_L} \right) + 5 \log \left(\frac{3T}{m_{H^0} + 2M} \right) + \frac{M^2 - 2m_{H^0}^2}{M^2} \log \left(\frac{m_{H^0} + M}{m_{H^0} + 2M} \right) \right\} \\
\delta V_{log}^{(m+n)} &= \frac{g^2}{64\pi^2} T^2 \left[33M^2 \log \left(\frac{T}{M} \right) - 6(M^2 - 4M_L^2) \log \left(\frac{3T}{2M_L + M} \right) \right] \quad (C.3)
\end{aligned}$$

$$\begin{aligned}
\delta V_{log}^{(p)} &= -\frac{g^4}{64\pi^2} \frac{T^2}{16} \left\{ 3c_{2r}^2 \left[\varphi_{cos}^2 \log \left(\frac{T}{m_{h^0}} \right) + \varphi_{sin}^2 \log \left(\frac{T}{m_{H^0}} \right) \right] \right. \\
&+ 2(\varphi_v - s_{2c}\varphi_{sin})^2 \log \left(\frac{3T}{m_{h^0} + 2m_{G^\pm}} \right) + 2(\varphi_0 - s_{2c}\varphi_{cos})^2 \log \left(\frac{3T}{m_{H^0} + 2m_{G^\pm}} \right) \\
&+ 2(\varphi_v + s_{2c}\varphi_{sin})^2 \log \left(\frac{3T}{m_{h^0} + 2m_{H^\pm}} \right) + 2(\varphi_0 + s_{2c}\varphi_{cos})^2 \log \left(\frac{3T}{m_{H^0} + 2m_{H^\pm}} \right) \\
&+ 4c_{2c}^2 \left[\varphi_{sin}^2 \log \left(\frac{3T}{m_{h^0} + m_{G^\pm} + m_{H^\pm}} \right) + \varphi_{cos}^2 \log \left(\frac{3T}{m_{H^0} + m_{G^\pm} + m_{H^\pm}} \right) \right] \\
&+ 4 \left[\varphi_{0,i}^2 \log \left(\frac{3T}{m_{G^0} + m_{G^\pm} + m_{H^\pm}} \right) + \varphi_{v,i}^2 \log \left(\frac{3T}{m_{A^0} + m_{G^\pm} + m_{H^\pm}} \right) \right] \\
&+ (2\varphi_0 - 3c_{2r}\varphi_{sin})^2 \log \left(\frac{3T}{m_{H^0} + 2m_{h^0}} \right) + (2\varphi_v - 3c_{2r}\varphi_{cos})^2 \log \left(\frac{3T}{2m_{H^0} + m_{h^0}} \right) \\
&+ c_{2i}^2 \left(\varphi_{cos}^2 \left[\log \left(\frac{3T}{m_{h^0} + 2m_{G^0}} \right) + \log \left(\frac{3T}{m_{h^0} + 2m_{A^0}} \right) \right] \right. \\
&+ \left. \varphi_{sin}^2 \left[\log \left(\frac{3T}{m_{H^0} + 2m_{G^0}} \right) + \log \left(\frac{3T}{m_{H^0} + 2m_{A^0}} \right) \right] \right) \\
&+ \left. 2s_{2i}^2 \left[\varphi_{cos}^2 \log \left(\frac{3T}{m_{h^0} + m_{G^0} + m_{A^0}} \right) + \varphi_{sin}^2 \log \left(\frac{3T}{m_{H^0} + m_{G^0} + m_{A^0}} \right) \right] \right\} \quad (C.4)
\end{aligned}$$

and including squarks:

$$\begin{aligned}
\delta V_{log}^{(a')} &= -\frac{g^2}{128\pi^2} T^2 N_c \left\{ 4(M^2 - 2m_{\tilde{t}_L}^2 - 2m_{\tilde{b}_L}^2) \log \left(\frac{3T}{m_{\tilde{t}_L} + m_{\tilde{b}_L} + M} \right) \right. \\
&+ 4 \frac{(m_{\tilde{t}_L}^2 - m_{\tilde{b}_L}^2)^2}{M^2} \log \left(\frac{m_{\tilde{t}_L} + m_{\tilde{b}_L}}{m_{\tilde{t}_L} + m_{\tilde{b}_L} + M} \right) \\
&+ (M^2 - 4m_{\tilde{t}_L}^2) \log \left(\frac{3T}{2m_{\tilde{t}_L} + M} \right) + (M^2 - 4m_{\tilde{b}_L}^2) \log \left(\frac{3T}{2m_{\tilde{b}_L} + M} \right) \left. \right\} \\
&+ \frac{g_s^2}{16\pi^2} T^2 (N_c^2 - 1) \left\{ m_{\tilde{t}_L}^2 \log \left(\frac{3T}{2m_{\tilde{t}_L}} \right) + m_{\tilde{b}_L}^2 \log \left(\frac{3T}{2m_{\tilde{b}_L}} \right) \right. \\
&+ \left. m_{\tilde{t}_R}^2 \log \left(\frac{3T}{2m_{\tilde{t}_R}} \right) + m_{\tilde{b}_R}^2 \log \left(\frac{3T}{2m_{\tilde{b}_R}} \right) \right\} \quad (C.5)
\end{aligned}$$

$$\delta V_{log}^{(p')} = -\frac{N_c}{32\pi^2} T^2 \left\{ (h_t^2 c_r \varphi_2)^2 \log \left(\frac{3T}{m_{h^0} + 2m_{\tilde{t}_R}} \right) + (h_t^2 s_r \varphi_2)^2 \log \left(\frac{3T}{m_{H^0} + 2m_{\tilde{t}_R}} \right) \right\}$$

$$\begin{aligned}
& + \left(h_t^2 c_r \varphi_2 - \frac{g^2}{4} \varphi_{\cos} \right)^2 \log \left(\frac{3T}{m_{h^0} + 2m_{\tilde{t}_L}} \right) + \left(h_t^2 s_r \varphi_2 + \frac{g^2}{4} \varphi_{\sin} \right)^2 \log \left(\frac{3T}{m_{H^0} + 2m_{\tilde{t}_L}} \right) \\
& + \left(\frac{g^2}{4} \varphi_{\cos} \right)^2 \log \left(\frac{3T}{m_{h^0} + 2m_{\tilde{b}_L}} \right) + \left(\frac{g^2}{4} \varphi_{\sin} \right)^2 \log \left(\frac{3T}{m_{H^0} + 2m_{\tilde{b}_L}} \right) \\
& + \left(h_t^2 c_c \varphi_2 - \frac{g^2}{2} \varphi_{\cos,c} \right)^2 \log \left(\frac{3T}{m_{G^\pm} + m_{\tilde{t}_L} + m_{\tilde{b}_L}} \right) \\
& + \left. \left(h_t^2 s_c \varphi_2 - \frac{g^2}{2} \varphi_{\sin,c} \right)^2 \log \left(\frac{3T}{m_{H^\pm} + m_{\tilde{t}_L} + m_{\tilde{b}_L}} \right) \right\} \quad (C.6)
\end{aligned}$$

The linear terms needed to insure $\partial V/\partial\varphi_1 = \partial V/\partial\varphi_2 = 0$ at $\varphi_1 = \varphi_2 = 0$ are

$$\delta V_{lin}^{(a)} = -\frac{3}{8} g^2 M (m_{h^0} + 2m_{G^\pm} + m_{G^0} + m_{H^0} + 2m_{H^\pm} + m_{A^0}) \frac{T^2}{16\pi^2}, \quad (C.7)$$

$$\delta V_{lin}^{(b)} = \frac{3}{64} g^4 \frac{1}{M} (\varphi_v^2 m_{h^0} + \varphi_0^2 m_{H^0}) \frac{T^2}{8\pi^2}, \quad (C.8)$$

$$\delta V_{lin}^{(c)} = -2\delta V_{lin}^{(a)}, \quad (C.9)$$

$$\delta V_{lin}^{(m+o)} = 3g^2 M M_L \frac{T^2}{16\pi^2}, \quad (C.10)$$

and

$$\delta V_{lin}^{(a')} = -g^2 N_c \frac{3M}{2} (m_{\tilde{t}_L} + m_{\tilde{b}_L}) \frac{T^2}{32\pi^2} \quad (C.11)$$

$$\delta V_{lin}^{(c')} = 3g^2 N_c M (m_{\tilde{t}_L} + m_{\tilde{b}_L}) \frac{T^2}{32\pi^2}. \quad (C.12)$$

It can be easily checked that ($i = 1, 2$)

$$\left. \frac{\partial}{\partial\varphi_i} \left(\delta V_{log+lin}^{(a)} + \delta V_{lin}^{(c)} \right) \right|_{\varphi=0} = 0,$$

a similar relation for ($a' + c'$), and

$$\left. \frac{\partial}{\partial\varphi_i} \left(\delta V_{log+lin}^{(m+o)} + \delta V_{log}^{(b+n)} \right) \right|_{\varphi=0} = 0.$$

The non-logarithmic terms involving only g_s and h_t couplings are:

For Standard Model diagrams

$$\delta V^{(i+j)} = \frac{m_t^2 T^2}{64\pi^2} \left[16g_s^2 \left(\frac{5}{3} \log 2 - \frac{1}{2} - c_B \right) + 3N_c h_t^2 \left(\frac{5}{3} \log 2 - c_B \right) \right], \quad (C.13)$$

with $c_B = \log(4\pi) - \gamma_E$, and from (B.2)

$$\delta V_{count} = \frac{m_t^2 T^2}{64\pi^2} (16g_s^2 - 3h_t^2) \log 2. \quad (\text{C.14})$$

Diagrams involving squarks give

$$\begin{aligned} \delta V^{(a')} &= -\frac{g_s^2 T^2}{64\pi^2} (N_c^2 - 1)(c_2 - 1)(m_{\tilde{t}_L}^2 + m_{\tilde{t}_R}^2), \\ \delta V^{(c')} &= \frac{g_s^2 T^2}{32\pi^2} (N_c^2 - 1) \left[\Pi_{gL}^{1/2}(m_{\tilde{t}_L} + m_{\tilde{t}_R}) + \frac{1}{6}(m_{\tilde{t}_L}^2 + m_{\tilde{t}_R}^2) \right] + \delta_{c_B} V^{(c')}, \\ \delta V^{(p')} &= \frac{3N_c T^2}{128\pi^2} c_2 h_t^4 \varphi_2^2, \\ \delta V^{(z')} &= \frac{N_c T^2}{32\pi^2} h_t^2 \left[(m_{\tilde{t}_L} + m_{\tilde{t}_R})(c_r^2 m_{h^0} + s_r^2 m_{H^0} + s_i^2 m_{A^0} + c_i^2 m_{G^0}) \right. \\ &\quad \left. + 2(m_{\tilde{t}_R} + m_{\tilde{b}_L})(c_c^2 m_{G^\pm} + s_c^2 m_{H^\pm}) \right] + \delta_{c_B} V^{(z')}, \\ \delta V^{(z'')} &= \frac{N_c T^2}{16\pi^2} \left[\frac{g_s^2}{6} (N_c + 1)(m_{\tilde{t}_L}^2 + m_{\tilde{t}_R}^2) + h_t^2 m_{\tilde{t}_R} (m_{\tilde{t}_L} + m_{\tilde{b}_L}) \right] + \delta_{c_B} V^{(z'')}, \end{aligned} \quad (\text{C.15})$$

with $c_2 \simeq 3.3025$.

The terms $\delta_{c_B} V$ add up to

$$\delta_{c_B} V = \frac{c_B}{16\pi^2} \sum_{i, \text{scalars}} n_i m_i^2 \Pi_i.$$

The contribution from thermal counterterms, eq. (B.3), gives exactly the same but with opposite sign so that they cancel out. If resummation of scalars is implemented only on zero Matsubara modes, there are no thermal counterterms. In that case $\delta_{c_B} V$ combines with the one-loop unresummed scalar contribution

$$\frac{c_B}{32\pi^2} \sum_i n_i m_i^4, \quad (\text{C.16})$$

to give

$$\frac{c_B}{32\pi^2} \sum_i n_i \overline{m}_i^4. \quad (\text{C.17})$$

That is precisely the one-loop result if we resum all modes, so that after the cancellation of two-loop contributions and thermal counterterms, both resummation methods give the same result. This is no longer true in the presence of particle mixing (this occurs in our case in the Higgs sector) where a small numerical difference is expected.

References

- [1] A.G. Cohen, D.B. Kaplan and A.E. Nelson, *Ann. Rev. Nucl. Part. Sci.* 43 (1993) 27; M. Quirós, *Helv. Phys. Acta* 67 (1994) 451; V.A. Rubakov and M.E. Shaposhnikov, *Phys. Usp.* 39 (1996) 461 [hep-ph/9603208].
- [2] W. Buchmüller, Preprint DESY 96-216, [hep-ph/9610335].
- [3] See e.g. H.P. Nilles, *Phys. Rep.* 110 (1984) 1; H.E. Haber and G.L. Kane, *Phys. Rep.* 117 (1985) 75; H. Baer et al. Preprint FSU-HEP-950401 [hep-ph/9503479]; M. Drees and S.P. Martin, Report of Subgroup 2 of the DPF Working Group on ‘Electroweak Symmetry Breaking and Beyond the Standard Model’ [hep-ph/9504324].
- [4] S. Davidson and R. Hempfling, *Phys. Lett.* B391 (1997) 287.
- [5] M. Pietroni, *Nucl. Phys.* B402 (1993) 27; A.T. Davies, C.D. Froggatt and R.G. Moorhouse, *Phys. Lett.* B372 (1996) 88.
- [6] For review and references see: Y. Grossman, Y. Nir and R. Rattazzi, Preprint SLAC-PUB-7379 [hep-ph/9701231].
- [7] P. Huet and A. Nelson, *Phys. Lett.* B355 (1995) 229; *Phys. Rev.* D53 (1996) 4578.
- [8] D. Comelli, M. Pietroni and A. Riotto, *Phys. Lett.* B354 (1995) 91; *Phys. Rev.* D53 (1996) 4668; A. Riotto, *Phys. Rev.* D53 (1996) 5834.
- [9] M. Carena, M. Quirós, A. Riotto, I. Vilja and C.E.M. Wagner, Preprint CERN-TH/96-242 [hep-ph/9702409].
- [10] M.P. Worah, Preprint SLAC-PUB-7417 [hep-ph/9702423].
- [11] P. Arnold, D. Son and L. Yaffe, Preprint UW-PT-96-19 [hep-ph/9609481]; P. Arnold, Preprint UW-PT-97-2 [hep-ph/9701393].
- [12] P. Huet and D.T. Son, Preprint UW-PT-96-20 [hep-ph/9610259].
- [13] A.V. Smilga, Preprint TPI-MINN-96-23 [hep-ph/9612347].
- [14] D. Comelli and M. Pietroni, *Phys. Lett.* B306 (1993) 67; J.R. Espinosa, J.M. Moreno and M. Quirós, *Phys. Lett.* B319 (1993) 505; D. Comelli, M. Pietroni and A. Riotto, *Nucl. Phys.* B412 (1994) 441.
- [15] A. Pomarol, *Phys. Lett.* B272 (1991) 313.
- [16] M.E. Shaposhnikov *JETP Lett.* 44 (1986) 465; *Nucl. Phys.* B287 (1987) 757.
- [17] G.F. Giudice, *Phys. Rev.* D45 (1992) 3177.
- [18] S. Myint, *Phys. Lett.* B287 (1992) 325.

- [19] J.R. Espinosa, M. Quirós and F. Zwirner, Phys. Lett. B307 (1993) 106.
- [20] A. Brignole, J.R. Espinosa, M. Quirós and F. Zwirner, Phys. Lett. B324 (1994) 181.
- [21] M. Carena, M. Quirós and C.E.M. Wagner, Phys. Lett. B380 (1996) 81.
- [22] J.R. Espinosa, Nucl. Phys. B475 (1996) 273.
- [23] D. Delepine, J.M. Gerard, R. González Felipe and J. Weyers, Phys. Lett. B386 (1996) 183.
- [24] J.R. Espinosa, in Electroweak Physics and the Early Universe, NATO ASI Series B: Physics Vol. 338 p.93 (Edits. J. C. Romao and F. Freire) Plenum Press (1994).
- [25] M. Laine, Nucl. Phys. B481 (1996) 43.
- [26] M. Losada, Preprint RU-96-25 [hep-ph/9605266] and [hep-ph/9612337]; G. Farrar and M. Losada, Preprint RU-96-26 [hep-ph/9612346].
- [27] J.M. Cline and K. Kainulainen, Nucl. Phys. B482 (1996) 73.
- [28] P. Ginsparg, Nucl. Phys. B170 (1980) 388; T. Appelquist and R. Pisarski, Phys. Rev. D23 (1981) 2305; S. Nadkarni, Phys. Rev. D27 (1983) 917.
- [29] A. Jakovác, K. Kajantie and A. Patkós, Phys. Rev. D49 (1994) 6810; K. Farakos, K. Kajantie, K. Rummukainen and M.E. Shaposhnikov, Nucl. Phys. B425 (1994) 67; K. Kajantie, M. Laine, K. Rummukainen and M.E. Shaposhnikov, Nucl. Phys. B458 (1996) 90.
- [30] J.M. Cline, private communication.
- [31] W. Buchmüller and O. Philipsen, Preprint DESY 96-241 [hep-ph/9612286]; B. Bergerhoff and C. Wetterich, Preprint HD-THEP-96-51 [hep-ph/9611462].
- [32] J.R. Espinosa, M. Quirós and F. Zwirner, Phys. Lett. B314 (1993) 206; W. Buchmüller, Z. Fodor, T. Helbig and D. Walliser, Ann. Phys. 234 (1994) 260.
- [33] W. Buchmüller and O. Philipsen, Nucl. Phys. B443 (1995) 403.
- [34] K. Kajantie, M. Laine, K. Rummukainen and M.E. Shaposhnikov, Phys. Rev. Lett. 77 (1996) 2887.
- [35] Y. Okada, M. Yamaguchi and T. Yanagida, Prog. Theor. Phys. Lett. 85 (1991) 1 and Phys. Lett. B262 (1991) 54; J. Ellis, G. Ridolfi and F. Zwirner, Phys. Lett. B257 (1991) 83; H.E. Haber and R. Hempfling, Phys. Rev. Lett. 66 (1991) 1815; R. Barbieri and M. Frigeni, Phys. Lett. B258 (1991) 395.
- [36] G. Anderson and L. Hall, Phys. Rev. D45 (1992) 2685.

- [37] P. Arnold and O. Espinosa, Phys. Rev. D47 (1993) 3546; ERRATUM-ibid. D50 (1994) 6662.
- [38] J.M. Moreno, D.H. Oaknin and M. Quirós, Nucl. Phys. B483 (1997) 267.
- [39] R. Parwani, Phys. Rev. D45 (1992) 4695.
- [40] D. Bödeker, P. John, M. Laine and M.G. Schmidt, Preprint HD-THEP-96-56 [hep-ph/9612364].
- [41] J.E. Bagnasco and M. Dine, Phys. Lett. B303 (1993) 308; Z. Fodor and A. Hebecker, Nucl. Phys. B432 (1994) 127; W. Buchmüller, Z. Fodor, A. Hebecker, Nucl. Phys. B447 (1995) 317.
- [42] D. Comelli and J.R. Espinosa, Preprint DESY 96-114 [hep-ph/9606438] to be published in Phys. Rev. D.